공학박사학위논문

거친 표면에 인터로크를 위한 금속 미세 핀 배열의 가공

Fabrication of Metal Micro-pin Array for Mechanical Interlocking on Rough Surface

2014년 2월

서울대학교 대학원

기계항공공학부

이 세 원

FABRICATION OF MICRO-PIN ARRAY FOR MECHANICAL INTERLOCKING ON ROUGH SURFACE

DISSERTATION

SUBMITTED TO THE SCHOOL OF MECHANICAL

AND AEROSPACE ENGINEEERING AND THE COMMITTEE ON

GRADUATE STUDIES OF SEOUL NATIONAL UNIVERSITY

IN PARTIAL FULFILLMENT OF THE REQUIREMENTS

FOR THE DEGREE OF DOCTOR OF PHILOSOPHY

Se Won Lee

October 2013

거친 표면에 인터로크를 위한 금속 미세 핀 배열의 가공

Fabrication of Metal Micro-pin Array for Mechanical Interlocking on Rough Surface

지도교수 주 종 남

이 논문을 공학박사 학위논문으로 제출함

2013년 10월

서울대학교 대학원

기계항공공학부

이 세 원

이세원의 공학박사 학위논문을 인준함

2013년 12월

위 원 장 : _____

부위원장 : _____

위 원 : _____

위 원 : _____

위 원 : _____

Abstract

Se Won Lee

School of Mechanical and Aerospace Engineering

The Graduate School

Seoul National University

In this research, fabrication of metal micro-pin array for mechanical interlocking on rough surface was carried out. Nanosecond pulsed laser beam machining which has advantages for large area machining was applied and the machining methods that appropriate to the machining property of metals were proposed. In the case of stainless steel that has high viscosity and surface tension of its liquid state and that generates much dross and recast layer in laser beam machining process, dross and recast layer were piled for fabricating high aspect ratio micro-pin array. In the case of tungsten that is disadvantageous to precise machining using laser beam machining due to high melting point and high thermal conductivity, laser beam machining and electrochemical etching were used for fabricating micro-pin array. And the machining characteristics for each process were investigated according to machining parameters.

Fabricated micro-pin array was applied for interlocking on rough surface. The

interlocking force was measured according to micro-pin shape and rough surface conditions. The principle of micro-pin array interlocking on rough surface was investigated. Calculated force using interlocking model was compared with measured force. And interlocking force was estimated using surface profile and developed interlocking model. To increase applicability of micro-pin array interlocking, tilted micro-pin array and flexible base micro-pin array were developed. Tilted micro-pin array could generate more and directional interlocking force. Flexible base micro-pin array could interlock on curved rough surface.

Keywords: Metal micro-pin array, Precise machining, Laser beam machining, Electrochemical machining, Interlocking, Rough surface.

Student number: 2006-23098

Contents

List of Figures

outside force, (b) SEM image of flexible base micro-pin array

List of Tables

Chapter 1

Introduction

1.1 Research background

Recently, there has been much interest in the micro patterning on large area. Especially, the micro pattern of high aspect ratio like pin/pillar/column can contribute to micro electromechanical systems (MEMS), the field of bio-engineering and the robotics research field. In MEMS research, the micro-pin array can be applicable to micro fluidics as hydrodynamic chromatography [1, 2]. In bio-engineering research, it has much potential such as DNA separation, solar cells and super-hydrophobic surfaces [3-5]. And in robotics, it can be used for vertical wall attachment by interlocking on rough surface.

To increase the performance of robot, vertical wall attachment is important ability. The attachment mechanism to vertical surface is a currently active research field in robot mobility. The ability of attachment to vertical surface can increase the robot mobility and expand robot's working area. Various mechanisms

for attachment to vertical surface were proposed. For the smooth surface such as glass and interior walls, pneumatic suction cup [6, 7] or adhesive pad [8] have been employed to climb and attach to vertical wall. However, these methods are not applicable to rough, porous and dusty surface such as concrete, brick and exterior walls. Thus, for the unsmooth surface, the climbing robots have employed the spines or the claws [9-11]. The sharp tips on the spines or the claws can generate attachment force by engaging micro-asperities on the surface. For irregular surface, the robot uses their gripping device to climb the surface [12]. This kind of robot can also overcome vertical beam or wire netting wall. Recently, attaching method that inspired by Gecko is researched actively [13, 14]. It can attach to the vertical wall using Van der Waals force by means of compliant nano scale structure. Attaching method also depends on subject vertical wall property. On the iron wall, magnetic force can be used for attaching to vertical wall [15]. In the case of fabric wall, hook array (Velcro®) is applied [8].

Above methods are very useful, but the more research should be carried out due to the limitation of previous studies. First, each method has the range of optimal surface condition of subject plane. For example, magnetic force and hook array cannot be applied to the surface of appropriate material, iron or fabric. Attachment using spines cannot be applied to smooth surface like glass. On the other hand, mechanism using pneumatic suction cannot attach to rough surface. Figure 1.1

shows proper subject surfaces of existing mechanisms.

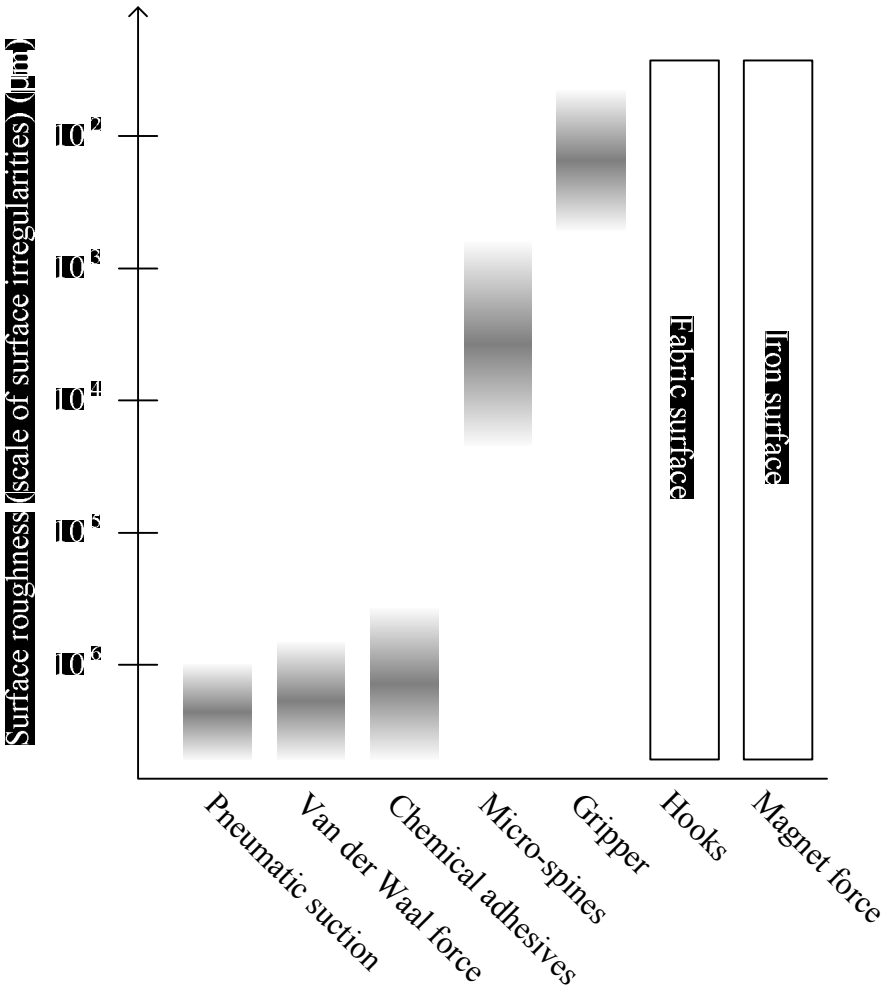

Figure 1.1 Proper subject surfaces of existing mechanisms

And the second limitation is expandability. Most of existing mechanism needs additional actuators and power supplies. They take up much space and weight. In the case of adhesive pad, durability problem occurs because the pad uses chemical adhesives.

The attachment by interlocking on rough surface using micro-pin array can be an alternative. The micro-pin array can interlock to the surface roughness from 10^{-6} meter to 10^{-4} meter. As shown in figure 1.1, the surface roughness of that range is not covered by existing mechanisms. In other words, the micro-pin array is the only application to specific surface roughness, for example interior wall. In addition, the micro-pin array needs no additional part because it is surface machining. So it has much expandability and applicability. And it can simplify the whole system.

In the case of the micro-pin array, the interlocking which is inspired by beetles on the rough surface is used [16]. The mechanism using micro-spines also adopts this principle. But the feature scale and the number of interlocking are completely different. The mechanism using micro-spines is that the sharp tips of the spines interlocks with the micro irregularities on the subject rough surface. Through this mechanism, the micro-spine should be sharp enough to attach to the fine surface because the irregularities on the fine surface are small. In addition, less force is generated for attachment on the small irregularities. It follows that existing robots

[10] which use spines are only able to interlock on rough surface walls like a concrete or brick wall because the spine tip is generally too large. In addition, to increase the chance to interlock, it needs compliant mechanism of foot. But in the case of the micro-pin array, the micro-pin is much smaller than the micro-spine. So it can interlock on the relatively fine surface by virtue of its sharp tip. In addition, it can increase chance to interlock due to the greater number of pins.

To manufacture a micro-pin array, various manufacturing processes have been proposed using photo electrochemical etching [17], photolithography [2], polydimethylsiloxane (PDMS) replication [18], and deep reactive ion etching (DRIE) [19]. However, these techniques have the disadvantage of high associated costs and a limitation on material applicability—they can only be used with polymer or silicon materials. Because the micro-pins have physical contact with the subject surface, the micro-pin array should have the appropriate mechanical property, like high elasticity, for attaching to a vertical wall. However, polymers have low stiffness, and silicon can easily be broken due to its high brittleness. For these reasons, polymer and silicon are not suitable materials for an attachment application. On the other hand, a metallic material could be a good candidate because of its mechanical properties.

Several machining technologies can be proposed to machine metallic materials. In particular, the non-traditional machining process can be applied to machine

micro products [20] . Micro electrical discharge machining (EDM) and micro electrochemical machining (ECM) have been researched for the micro-machining of metallic materials [21, 22]. These technologies are very precise, but they have a low machining speed. Therefore, they are not suitable for application in large area machining, such as in the fabrication of micro-pin arrays. On the other hand, laser beam machining (LBM) has large area machining capabilities due to its high machining speed. However, for example, a micro-pillar array was fabricated on a metallic alloy by laser-assisted surface modification, but the pins had an irregular shape and were tangled with neighboring pins [23]. For precise machining, an ultra-short pulsed laser beam, which has a pulse duration of picoseconds and femtoseconds, is generally used. But its material removal rate is so low that it is not suitable for large area machining. Thus, a machining process for micro-pin array fabrication, which has both machining speed and accuracy, is needed.

1.2 Research purpose and dissertation overview

The purpose of this study is the fabrication of the micro-pin array for interlocking on rough surface. To achieve this goal, nanosecond pulsed laser beam machining was used. Nanosecond pulsed laser beam machining has capability of high material remove rate on large area machining, but it has relatively low

machining quality comparing with ultra-short pulsed laser beam, which has a pulse duration of picoseconds and femtoseconds. To strengthen the strength and make up for the weakness of nanosecond pulsed laser beam machining, the appropriate machining processes according to the machining characteristic of each metallic material were developed. The principles of each machining processes were investigated theoretically and experimentally. Fabricated micro-pin array was used for interlocking on rough surface and the fabrication methods were developed for applications of micro-pin array. And the interlocking model was proposed and verified. This thesis is composed as follows.

In chapter 2, fabrication of micro-pin array using recast layer piling is presented. Machining process of the material (stainless steel, AISI 304) that generate much dross and recast layer in laser beam machining was presented. The laser beam machining system and the fabrication results according to laser beam machining conditions are introduced.

In chapter 3, fabrication of micro-pin array using laser beam machining and electrochemical etching is presented. Machining process of the material (tungsten) that has high thermal conductivity and no dross was presented. The experimental system for the process composed of electrochemical machining and laser beam machining are introduced and the machining characteristics according to machining condition are investigated.

In chapter 4, micro-pin array interlocking on rough surface is presented. Interlocking characteristics on rough surface are presented. In addition, principle of the micro-pin array interlocking on rough surface is presented. Micro-pin and rough surface interlocking modeling is established. And force estimation on a rough surface using modeling result is presented.

In chapter 5, applications of micro-pin array for interlocking were introduced. Fabrication method and its characteristics of tiled micro-pin array and flexible base micro-pin array are presented.

In chapter 6, conclusion and discussion of this study are presented.

Chapter 2

Fabrication of micro-pin array using recast layer piling

2.1 Laser beam machining of stainless steel (AISI 304)

Laser beam machining of stainless steel is not significantly different from carbon steel. The main difference is that stainless steel contains alloying element like chromium, nickel and so on. Especially, chromium element plays an important role to increase corrosion resistance of stainless steel. Chromium has higher reactivity than iron, so dense chromium oxide (Cr2O3) layer is generated on the surface before iron oxide [24, 25]. As a result, chromium oxide layer obstructs permeating of oxygen.

The generation of chromium oxide influences on laser beam machining of stainless steel. The metal generates heat of oxidation when it oxidizes. In laser beam machining process, the material is ablated by not only laser beam energy but also heat of oxidation. But in the case of stainless steel, chromium oxide obstructs

oxidation of iron. Furthermore, liquid state of chromium oxide has high viscosity and high surface tension [26]. Thus, melt chromium oxide is hard to be remove and augments the dross that remained on machining surface. Dross is the impurity floating on molten metal. In the case of stainless steel, chromium oxide is contained in the dross. As mentioned above, the dross, in the case of molten chromium oxide, is hard to ablate and remains on the machining surface due to its high surface tension and viscosity. Previous research showed that high viscosity molten metal reduces machining efficiency and machining quality in the laser beam process [27]. Since the dross obstructs the oxidation of iron by covering the reacting area, it also reduces laser machining efficiency. Thus, chromium oxide generation could be prevented by blowing a high pressured inert gas, such as nitrogen, or removed by an additional deburring process [26, 28-30].

Recast layer is also a factor that influences on laser beam machining of stainless steel. Especially in nanosecond pulsed laser beam machining, the recast layer as a burr is a major drawback. A nanosecond pulsed laser beam produces more recast layer than a picosecond and femtosecond pulsed laser due to the relatively long pulse. Because the short pulse laser beam can ablate the material before heat transfer, evidence of heat affection and a recast layer do not appear easily [26]. The recast layer, which forms around the machined area, causes low form accuracy. Therefore, the recast layer should be prevented and removed by a

general laser beam machining process for form accuracy.

2.2 Dross and recast layer piling

Dross and recast layer are the major weaknesses of nanosecond pulsed laser beam machining of stainless steel. In the process of this study, however, the recast layer and dross were not the targets of elimination, but rather utilized to fabricate a micro-pin array with a high aspect ratio by piling a recast layer. Stainless steel could be applied to this process due to its recast layer, which includes chromium oxide. As shown in figure 2.1 and figure 2.2, the high aspect ratio micro-pin array was fabricated by laser beam machining using the piling of a recast layer. As shown in figure 2.1, the pitch between the laser beam scanning paths was set slightly wider than the diameter of the laser beam spot. Zone A, between the laser beam scanning paths, was the remaining part after laser beam ablation. As a result, the recast layer was piled on zone A. In addition, the material in the spot area was not completely ablated due to laser beam pulse energy [24]. In the laser beam spot, there are various phenomena, for example, melting, ablation, and heat affection. The material had not completely evaporated, and therefore molten material was generated. The molten material was trapped on zone A, which was less influenced by the laser beam. Ultimately, the molten material was piled onto zone A and

solidified into a pin shape. Figure 2.2 shows a schematic diagram of the recast layer piling and combination procedure. First, the groove was machined onto the laser scanned area and the recast layer formed around the groove, as seen with recast layer 1 and 2. At a low scanning repeat count, the recast layer was of indeterminate shape. As the scanning repeat count increased, the recast layer piled continually. For the next step, the recast layers 1 and 2 piled more and overlapped with the contiguous recast layers. In this step, the recast layer flocked on zone A and combined into one as recast layer 1 + 2, as indicated in figure 2.2. Repeated scanning caused more recast layers, and a wider deeper groove. Finally, the recast layer was combined fully and formed a pin shape with a high aspect ratio. The height of the micro-pin was over the original metal surface because of the piled recast layer.

In the above process, the chromium oxide dross, which obstructed the laser ablation in the general laser beam machining process, played an important role. The high surface tension of the molten metal was difficult to ablate and keep in a molten state. As a result, the part that was covered by the recast layer was not ablated by the laser beam, and the micro-pins could maintain their shape and length.

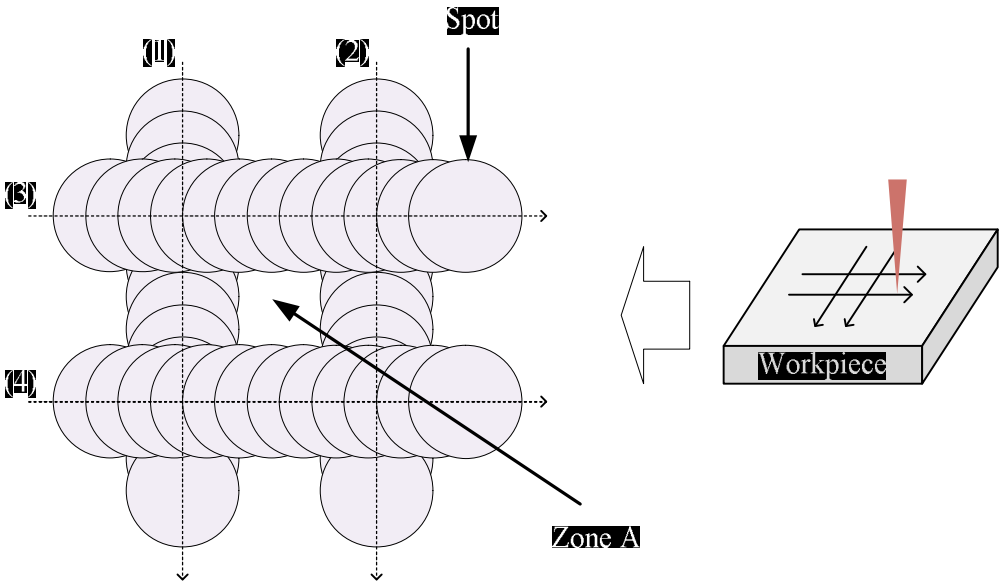

Figure 2.1 Pitch between scanning paths for piling of micro-pin arrays using combination of recast layers

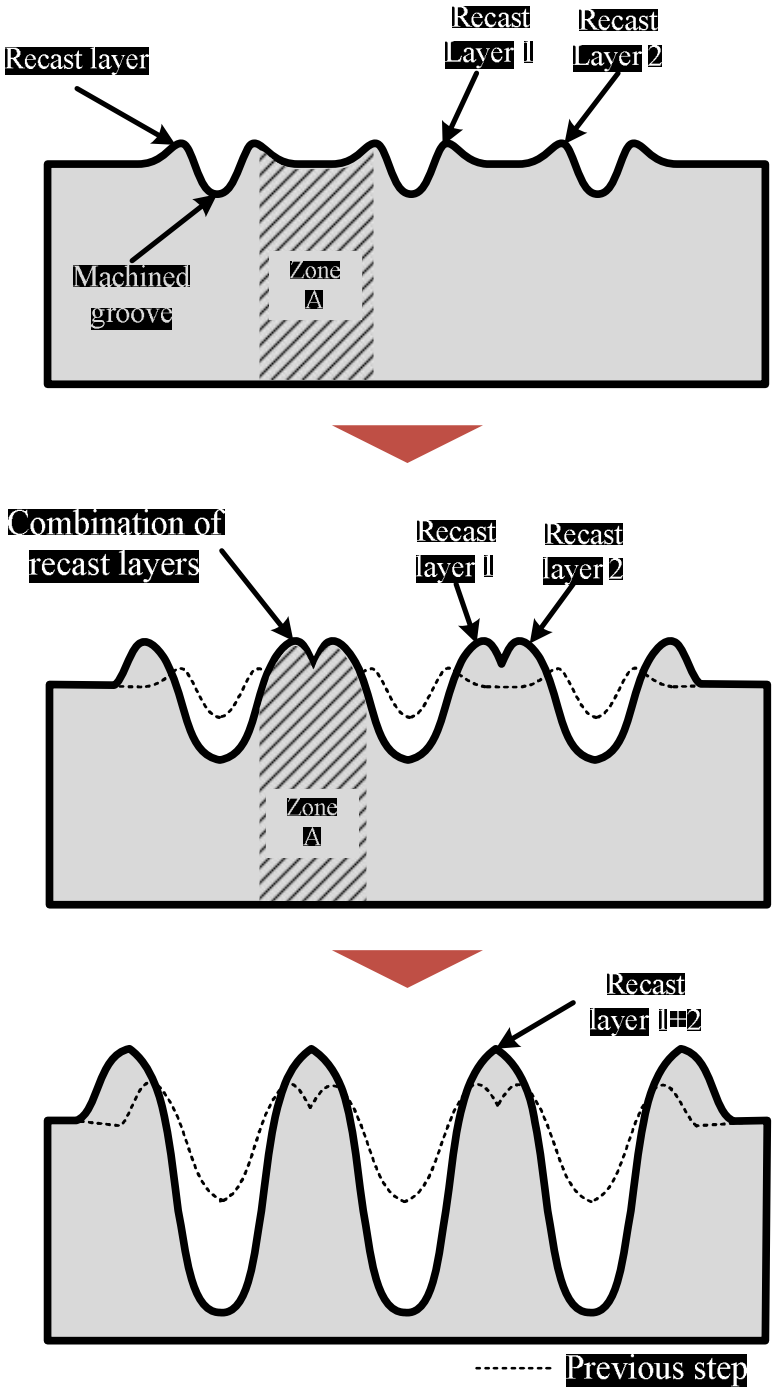

Figure 2.2 Procedure of recast layer piling and combination

2.3 System for laser beam machining

The main process of micro-pin array fabrication using recast layer piling is laser beam ablation by pulsed laser beam. An ytterbium fiber laser (IPG photonics, YLP-C series) with a 1064 nm wavelength was used. The pulsed laser repetition rate can be controlled from 20 kHz to 80 kHz, and the pulse width is 100 ns. The laser beam power was between 2.0 W and 8.0 W. The optically-calculated spot size was about 40 μm diameter [24], and the peak power density was from 1.0 kW/mm^2 to 4.0 kW/mm^2. The laser beam scan speed of the galvanometer was controlled from 108.6 mm/s to 408.6 mm/s. The galvanometer scan head (SCANLAB AG, SCANcube 10) was equipped on a Z-axis stage to set optical focal length. The schematics of the nanosecond pulsed laser beam machining system for the micro-pin array fabrication are shown in figure 2.3.

Stainless steel (AISI 304) of 0.5 mm thickness was used as a workpiece. The workpiece was polished with sandpaper and cleaned in acetone using ultrasonic cleaner. The component of AISI 304 stainless steel is indicated in table 2.1.

To investigate the machining results, scanning electron microscope (SEM) and X-ray photoelectron spectroscopy (XPS) were used.

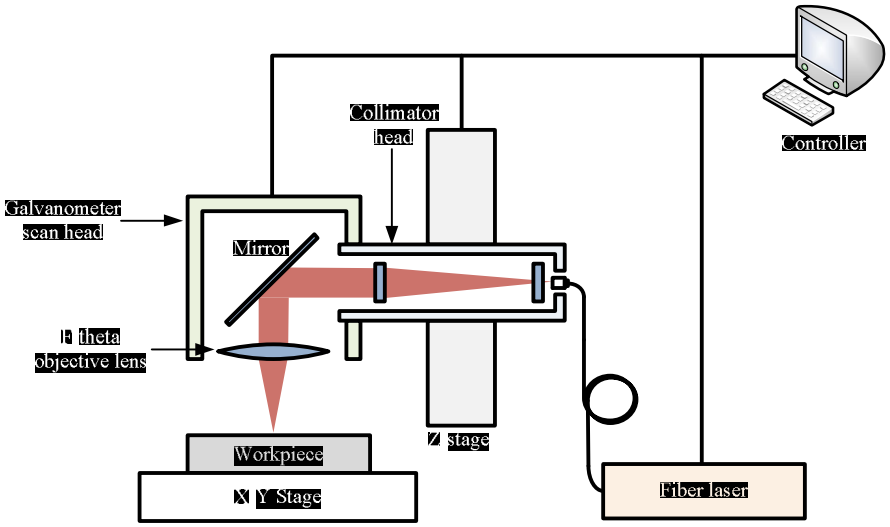

Figure 2.3 Experimental setup for fabricating micro-pin array using nanosecond pulsed laser beam machining

Table 2.1 Component of AISI stainless steel 304

Component elements properties	**Composition ratio**
Carbon, C	Under 0.080 %
Chromium, Cr	18.0 – 20.0 %
Iron, Fe	66.345 – 74.0 %
Manganese, Mn	Under 2.0%
Nickel, Ni	8.0 – 10.5 %
Phosphorous, P	Under 0.045 %
Silicon, Si	Under 1.0 %
Sulfur, S	Under 0.030 %

2.4 Fabrication of micro-pin array on stainless steel

The success of interlocking on rough surface is influenced by various conditions. A small pin tip radius increases the interlocking on rough surface. In addition, a long pin provides greater opportunity for the generation of an interlocking force. Figure 2.4 is a typical single line gird scanning path for fabricating a micro-pin array, and the scanning sequence of laser beam is also indicated; the horizontal lines were scanned before the vertical lines. The fabricated micro-pin array is indicated in figure 2.5.

The laser beam machining conditions were 2.5 kW/mm^2, 20 kHz frequency, 258.6 mm/s scan speed, and all the scanning path lines were repeated 2000 times. As a result, the pin shape from the single line path was not suitable for interlocking on rough surface because of short length and a narrow space between the pins. A micro-pin array with a narrow gap cannot be bent sufficiently due to the interrupt of neighboring pins. In addition, the micro-pin tip radius was too large. A micro-pin with a large radius tip has less chance of generating an attaching force. To solve the aforementioned problems, the laser beam scanning path and laser beam machining conditions should be investigated.

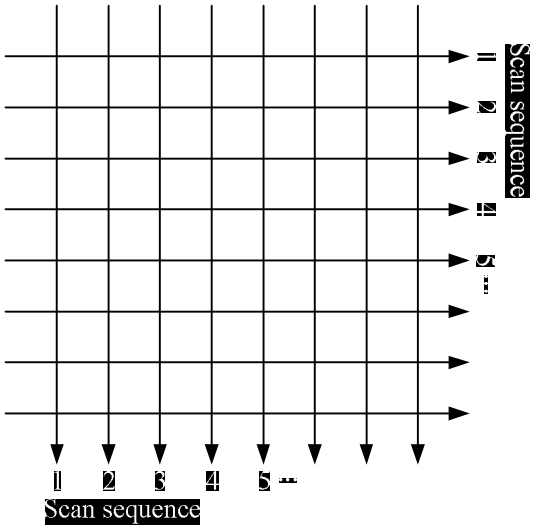

Figure 2.4 Typical single line gird scanning path for fabricating a micro-pin array and the scanning sequence

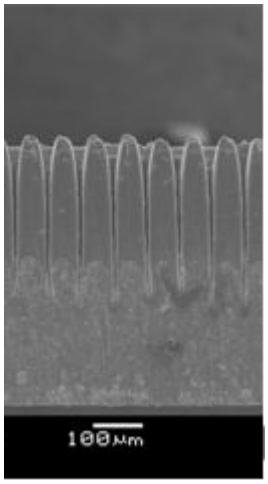

Figure 2.5 Fabricated micro-pin array using typical single line gird scanning path

2.4.1 Multi-line path of laser beam scanning

To solve the problems of a single line path, a multi-line scanning path indicated in figure 2.6 was applied. All of the laser beam machining conditions were the same except for the single line scanning path of figure 2.4. The multi-line scanning path was able to contribute to the pin length and the space between the pins. The laser beam machined groove was tapered generally, because the energy intensity of the laser beam had Gaussian distribution [31]. This means that the center of the laser beam spot had the highest energy intensity. It caused the depth limitation of the laser machined groove. The multi-line scanning path, composed of parallel lines with 10 μm line spacing, facilitated deeper and wider grooves by the overlapping of the laser beam spot.

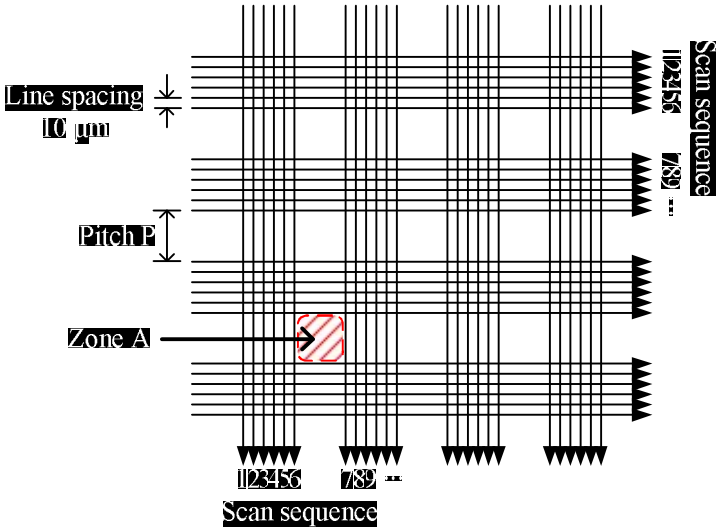

Figure 2.6 Multi-line scanning path for fabricating a micro-pin array and the scanning sequence

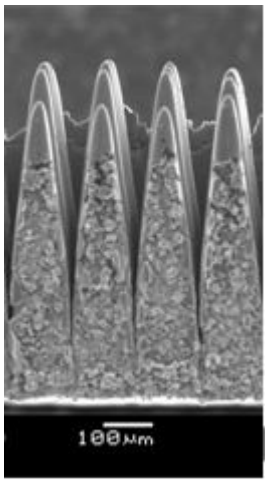

Figure 2.7 Fabricated micro-pin array using multi-line scanning path

As a result, the micro-pin length from the multi-line scanning paths was 603.1 μm. By comparison, the micro-pin length from single line path was 323.9 μm. Furthermore, the micro-pin array from the multi-line scanning path had a wide space between the pins. The pitch between the pins in figure 2.5 was narrow due to Gaussian distribution power intensity. On the other hand, the pitch between the pins in figure 2.7 became wider and deeper by overlapping the laser beam spot. In the case of the multi-line scanning path, the piled recast layer was also much more noticeable. As shown in figure 2.8 and 2.9, the multi-line scanning path was better in length and tip radius aspects. In the case of depth penetration, the multi-line path made a deeper groove than the single line path. In addition, the multi-line path made a wide groove and caused efficient material removal. The recast layer of the multi-line path was piled more than the single line path, and the quantity of removed material was furthermore increased because the depth penetration was greater. As a result, the length of the recast layer was relatively longer.

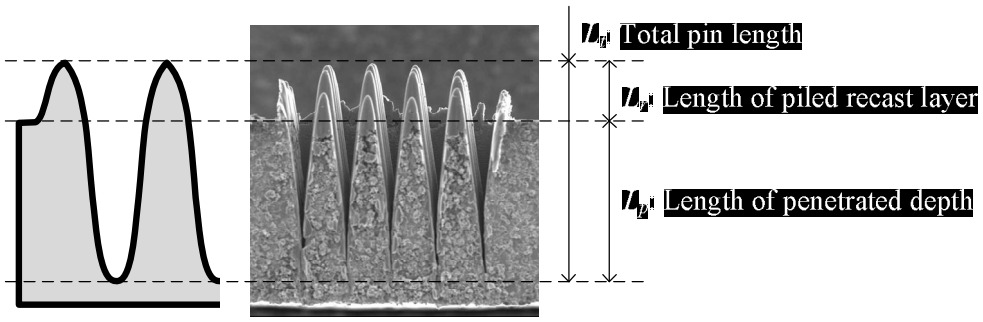

Figure 2.8 Schematic diagrams of micro-pin configuration. L_r is the length of piled recast layer and L_p is the length of penetrated depth. Total pin length L_t is the sum of L_r and L_p

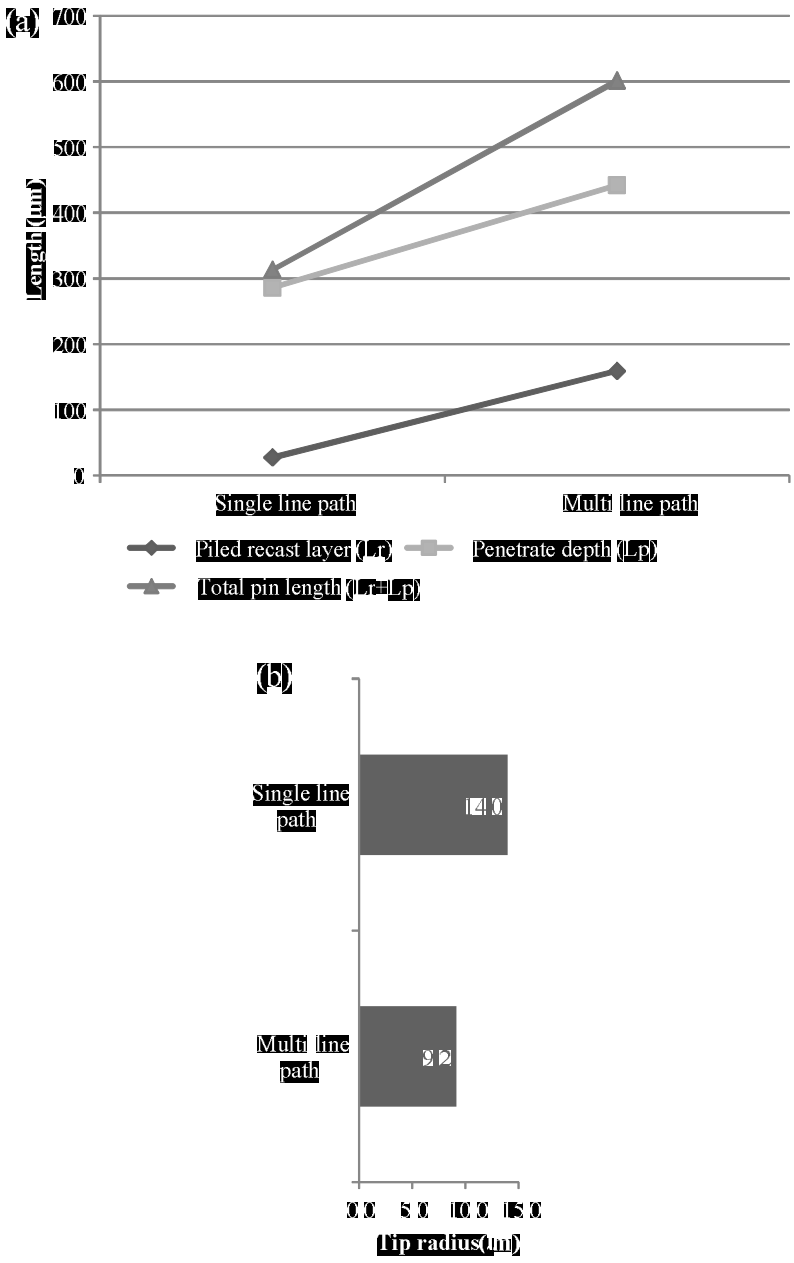

Figure 2.9 Micro-pin shape according to scanning path: (a) penetrate depth and recast layer length, (b) micro-pin tip radius

To detect the chromium oxide in the fabricated micro-pin array, X-ray photoelectron spectroscopy (XPS) analysis was used. Table 2.2 shows the binding energies of the different kinds of chromium oxide detected by the XPS analysis. As displayed in figure 2.10, the XPS spectrum of the fabricated micro-pin array surface shows the main peak on the binding energy of 576.8 eV. The XPS analysis results corresponded with the values in Table 1. Several states of chromium oxide were generated on the laser beam irradiated surface. Viewed in this result, the piled recast layer, including chromium oxide, assisted the micro-pin array fabrication during the laser beam process.

Table 2.2 Binding energies of the chemical states on chromium oxide

Chemical state	**Binding energy (eV)**
Cr_2O_3	576.9, 576.8
CrO_2	576.3

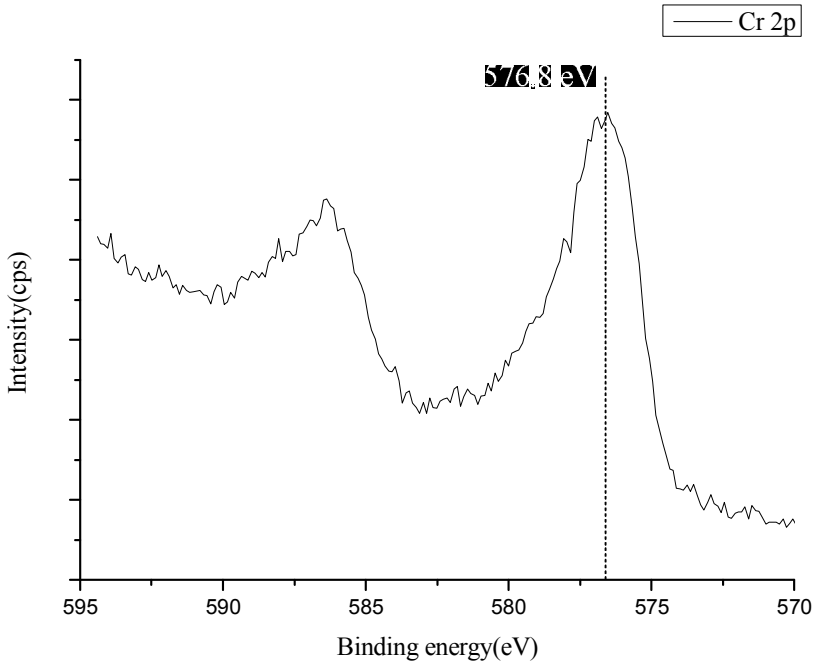

Figure 2.10 XPS spectra of micro-pin array surface about Cr 2p

2.4.2 Pitch of laser beam scanning path

Pitch P indicated in figure 2.6 determined the micro-pin tip shape. Pitch P is the distance between the multi-line groups. As pitch P became larger, the influence of the laser beam energy became weaker on zone A indicated in figure 2.6. By way of contrast, when pitch P was small, zone A received greater laser beam energy influence. The micro-pin shape according to pitch P is indicated in figure 2.11 and 2.12.

When pitch P was 46 μm, as shown in figure 2.11a and 2.11e, in the case of the small P, the micro-pin tip was sharp. But the micro-pin length was shortened due to the influence of laser beam ablation. Because pitch P was narrow, the laser beam energy could approach the center of zone A. As a result, part of zone A moved into the laser beam spot, and the recast layer piled on zone A was slightly ablated. On the other hand, in the case of a large pitch P of 65 μm, the uneven shape of the micro-pin was made, although the pin length was sufficient, as shown in figure 2.11c and 2.11g. When pitch P was excessively large, in the case of 75 μm, it could not form the pin tip, as indicated in figure 2.11d and 2.11h. The laser beam energy was too far from the center of zone A, hence the recast layer on the tip was not able to melt and combine completely. As a result, the recast layer was not able to engage properly and the micro-pin had cracks. Consequently, a proper range of pitch P was created in order to fabricate the micro-pin array by piling the

recast layer. In figure 2.11b and 2.11f, the micro-pin array was fabricated with 55 μm pitch P, which had a slightly larger value than the laser beam spot diameter. In this case, the pin length was 616.4 μm long. The recast layer was piled 146.5 μm, and the depth penetration was 469.8 μm. In addition, the fine and sharp tip was fabricated.

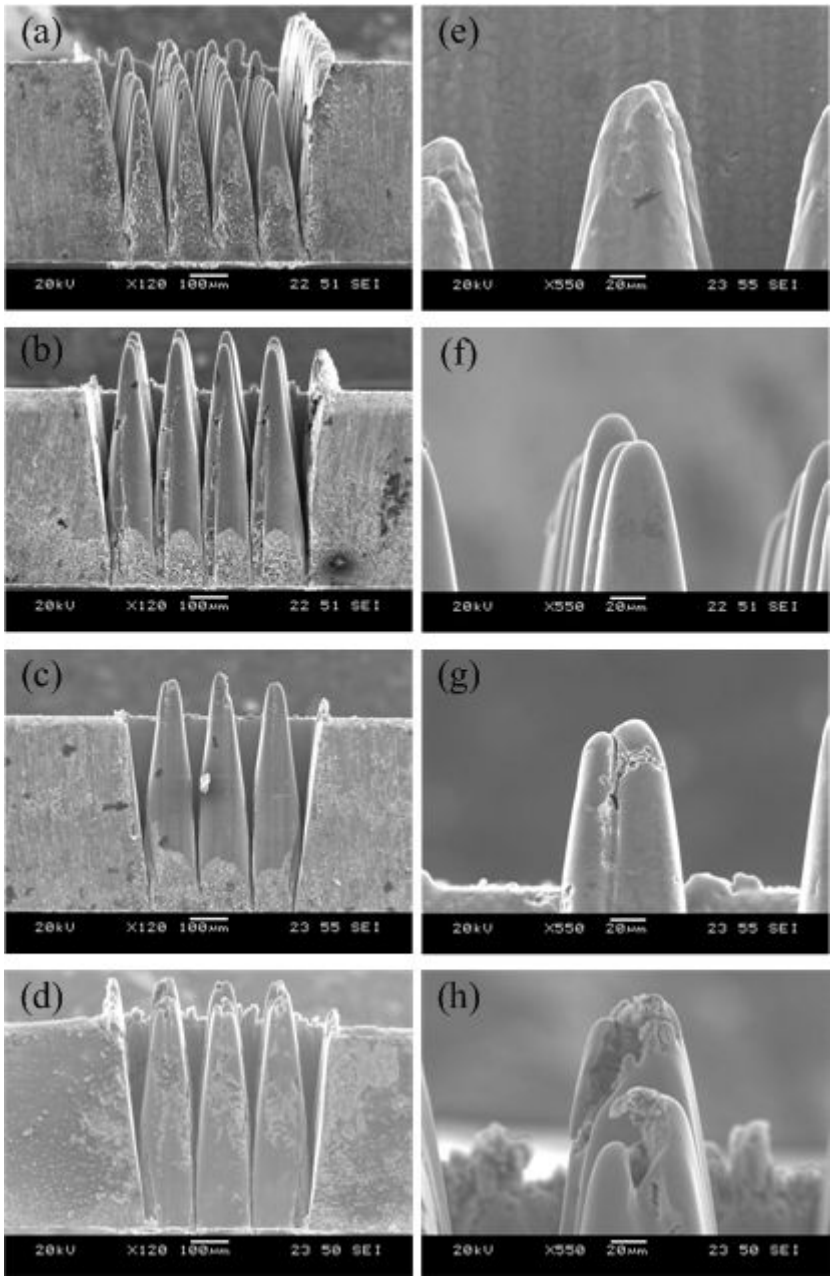

Figure 2.11 Micro-pin shape and enlarged picture of micro-pin tip according to pitch P: (a) and (e) 46 µm; (b) and (f) 55 µm; (c) and (g) 65 µm; (d) and (h) 75 µm

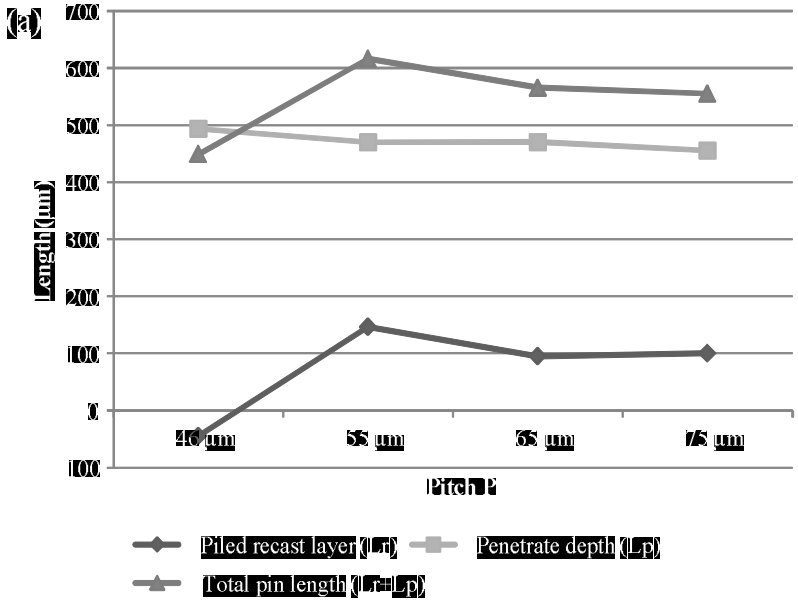

Figure 2.12 Micro-pin shape according to pitch P: (a) penetrate depth and recast layer length, (b) micro-pin tip radius

2.4.3 Peak power density

The peak power density influenced the micro-pin shape. The peak power density of the laser beam is defined by the average laser beam power and the area of the laser beam spot. The peak power density is the one of the primary factors in laser beam machining. In particular, peak power density is important in micro-pin array fabrication because it influences the machined groove shape and recast layer formation [24, 26, 31]. Figure 2.13 and 2.14 show the micro-pin shape change according to the peak power density. The other machining conditions were fixed at the multi-line scanning path, namely, 20 kHz frequency, 258.6 mm/s scan speed, and 2000 times scanning. In terms of the depth penetration, the groove was deep when the peak power density was high. However, over 3.3 kW/mm^2 of peak power density, the groove was so deep that the base of the micro-pin array was damaged and penetrated. As a result, the pins were completely ablated (figure 2.13). The length of the piled recast layer was also influenced by the peak power density. At the peak power density range of less than 2.5 kW/mm^2, the height of the piled recast layer was increased with the peak power density increase, as shown in figure 2.13a – 2.13c, and figure 2.14. In the case of 3.3 kW/mm^2, the length of the micro-pin was shortened because the laser beam affected the pin tip, as indicated in figure 2.13d. The laser beam energy near the border of the spot was relatively low according to the Gaussian distribution of the laser beam energy. In

this respect, the laser beam of low peak power density could not ablate the tip of the micro-pin [24]. But, at high peak power density, the tip of the micro-pin was influenced by the laser beam ablation. In this case, the tip of the micro-pin was laser ablated, and the length of the recast layer was shortened. In the case of 4.0 kW/mm^2 peak power density, the excessive peak power density eliminated all of the material in the machined area. Figure 2.14 shows the change in pin length and the depth penetration according to the peak power density. As a result, the machining condition of the peak power density range (2.5 – 3.3 kW/mm^2) was suitable for producing a micro-pin with a high aspect ratio.

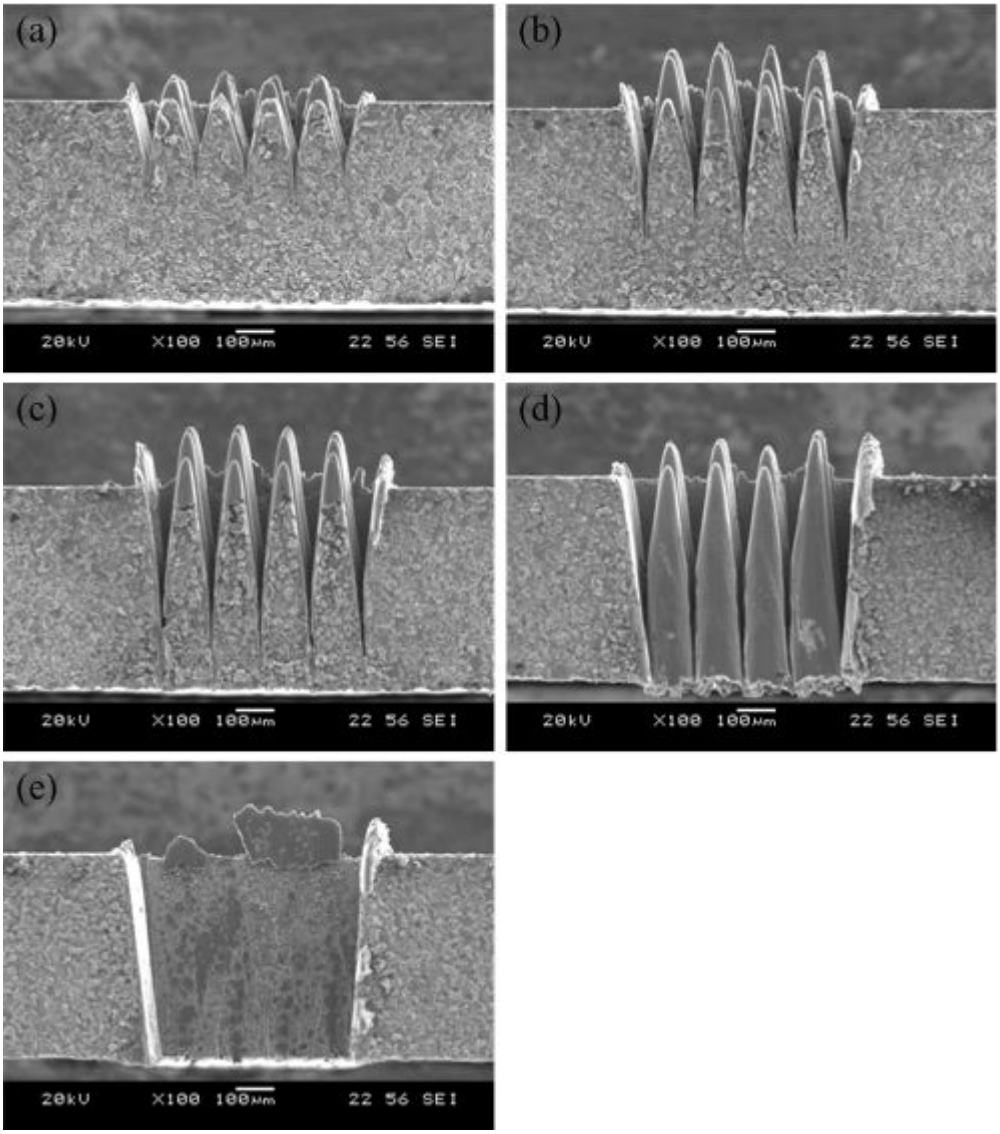

Figure 2.13 Micro-pin shape according to peak power density of laser beam: (a) 1.0 kW/mm^2, (b) 1.8 kW/mm^2, (c) 2.5 kW/mm^2, (d) 3.3 kW/mm^2, (e) 4.0 kW/mm^2

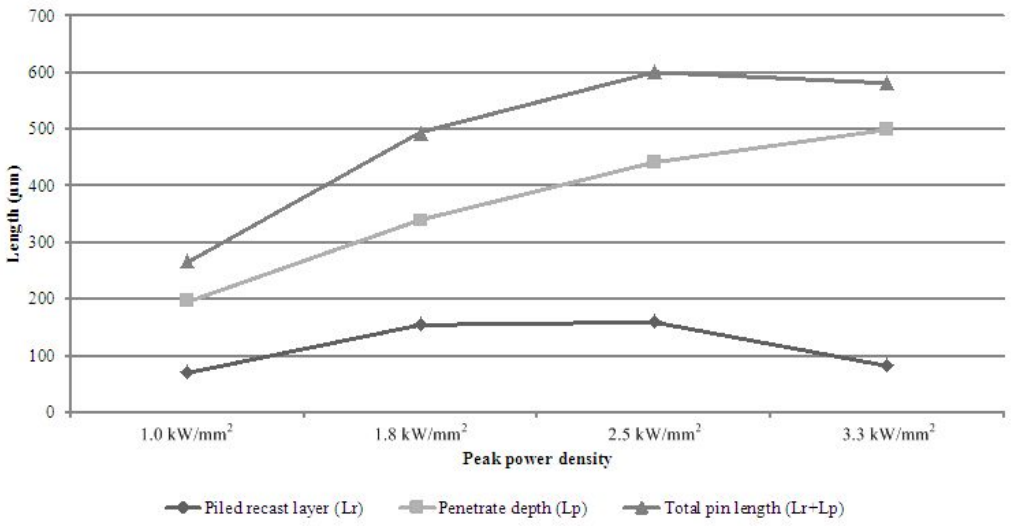

Figure 2.14 Penetrate depth and recast layer length of micro-pins according to peak power density

2.4.4 Laser beam scan speed

Scan speed can also influence micro-pin array fabrication. When the pulsed laser repetition rate is a fixed value, the scan speed and the interaction time are in inverse proportion to each other. In other words, the low scan speed causes a long interaction time. The long interaction time facilitates high material removal because the total laser beam energy on the unit area increases. Therefore, the micro-pin shape can be influenced by the laser beam scan speed. In figure 2.15 and 2.16, the effect of the scan speed was indicated in respect of the pin length and the tip radius. In those figures, depth penetration became low as the scan speed increased. The cause was a short interaction time. The micro-pin tip was ablated more at a low scan speed and long interaction time, because the workpiece was exposed to the laser beam for a greater period. As a result, it was completely penetrated in the lower scan speed condition of 108.6 mm/s, as shown in figure 2.15a. In addition, the length of the recast layer increased and converged as the scan speed increased. The length of the piled recast layer was influenced by the removed material quantity. At high scan speed, the removed material quantity reached the limit, and the length of the piled recast layer was converged. The pin tip radius, according to scan speed, is shown in figure 2.16b. It shows the same tendency with the length of the piled recast layer, because the pin tip was built up of the piled recast layer. Therefore, the pin tip radius was converged on the 258.6

mm/s scan speed in the same way as the pin length.

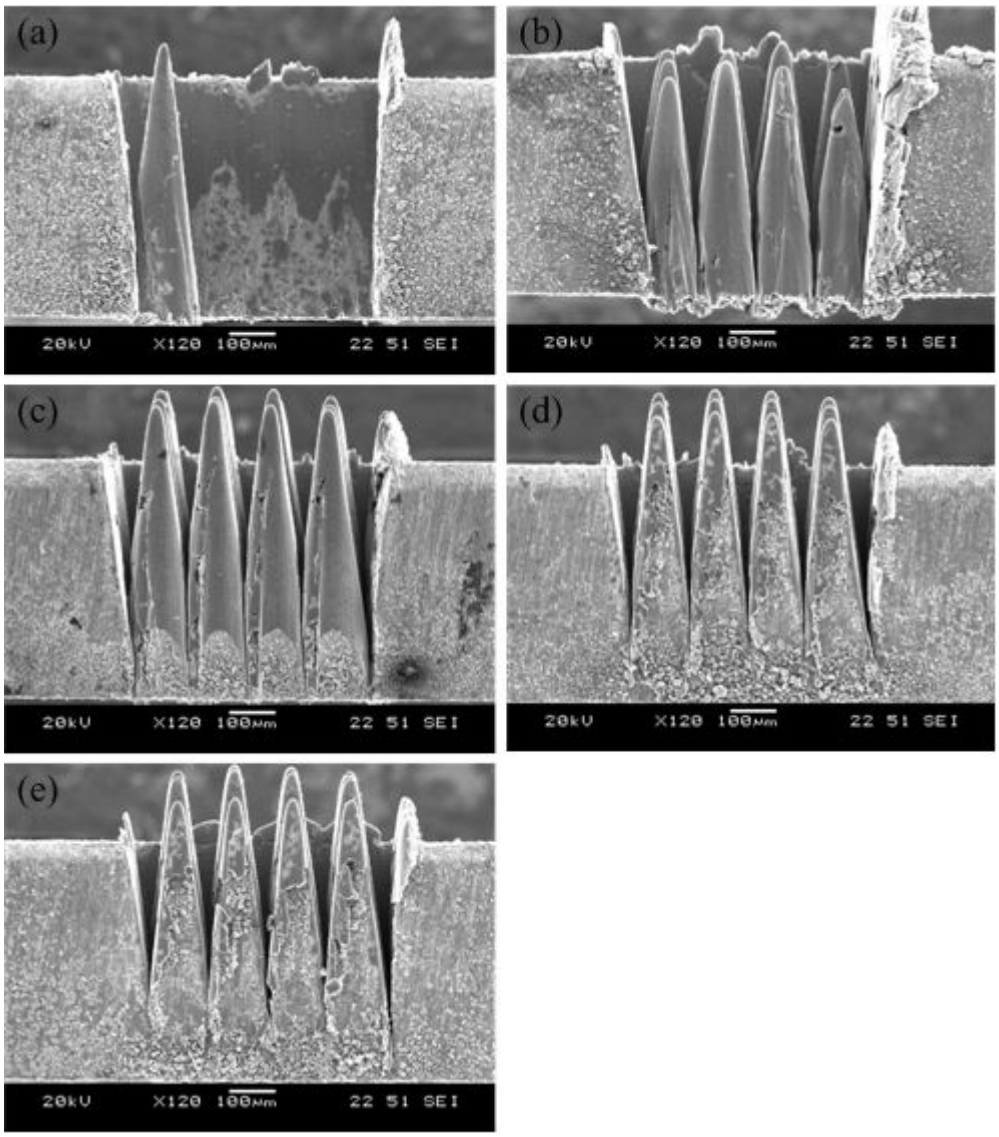

Figure 2.15 Micro-pin shape according to scan speed of laser beam: (a) 108.6 mm/s, (b) 158.6 mm/s, (c) 258.6 mm/s, (d) 358.6 mm/s, (e) 408.6 mm/s

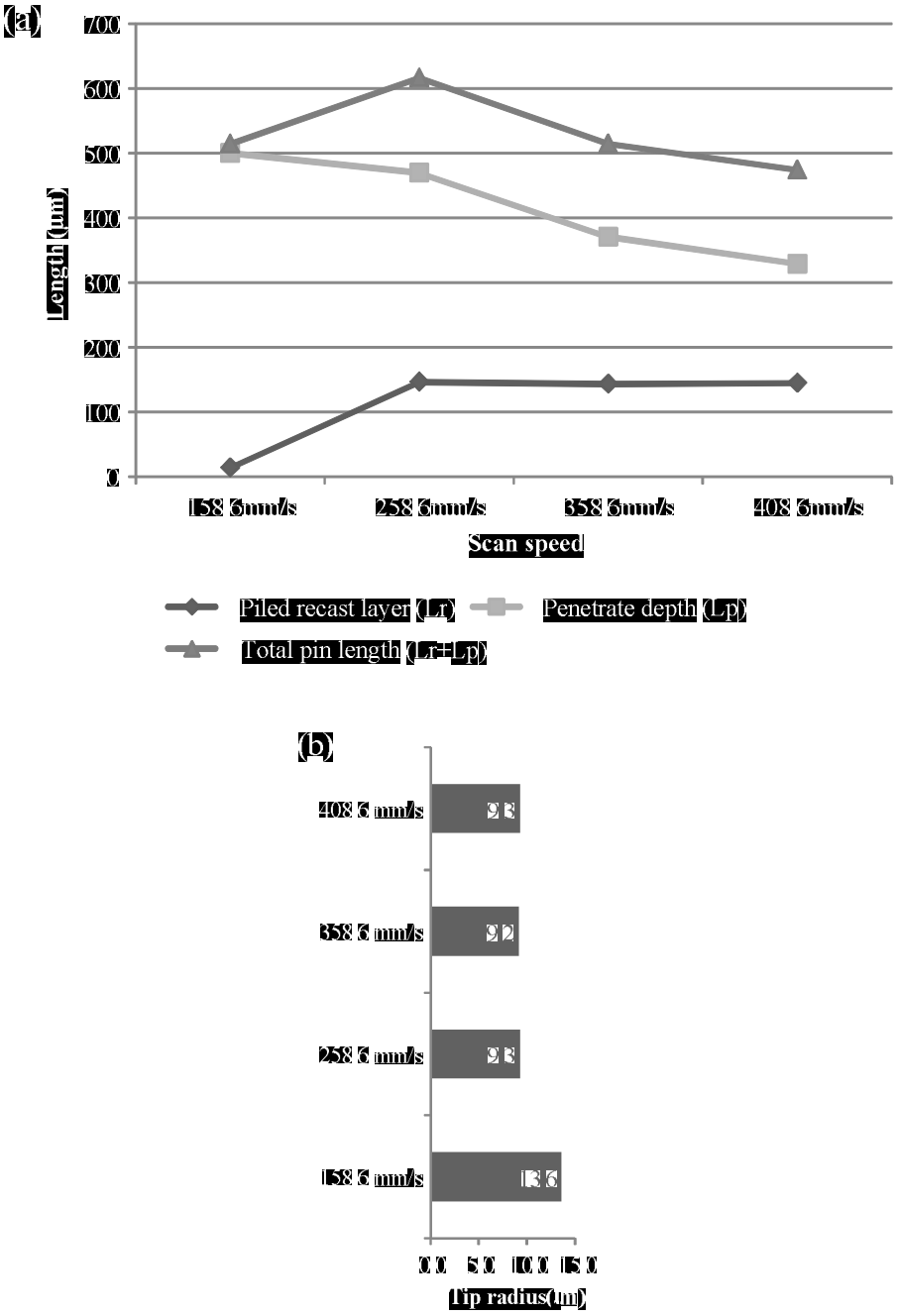

Figure 2.16 Micro-pin shape according to scan speed of laser beam: (a) penetrate depth and recast layer length, (b) micro-pin tip radius

2.4.5 The number of scanning repetition

The micro-pin array was fabricated using nanosecond pulsed laser beam machining. Figure 2.17 shows the recast layer piling with laser machining repetition. At the early phase of laser beam machining, just the laser-ablated mark and recast layer with irregular shape were in the laser beam-scanned area. When the scanning repeat count exceeded 10 times, the recast layer piled on zone A. The micro-pins became longer as the machining time increased. And the surface of the micro-pins became smooth due to the recast layer piling. As the machining progressed, the more the recast layer piled and the deeper the groove ablated. The picks of the pin tip rose over the original workpiece surface (over machining 100 times). The groove between the pins also became deep and wide. As a result, to fabricate a micro-pin array with a high aspect ratio, the scanning repeat count should be high enough.

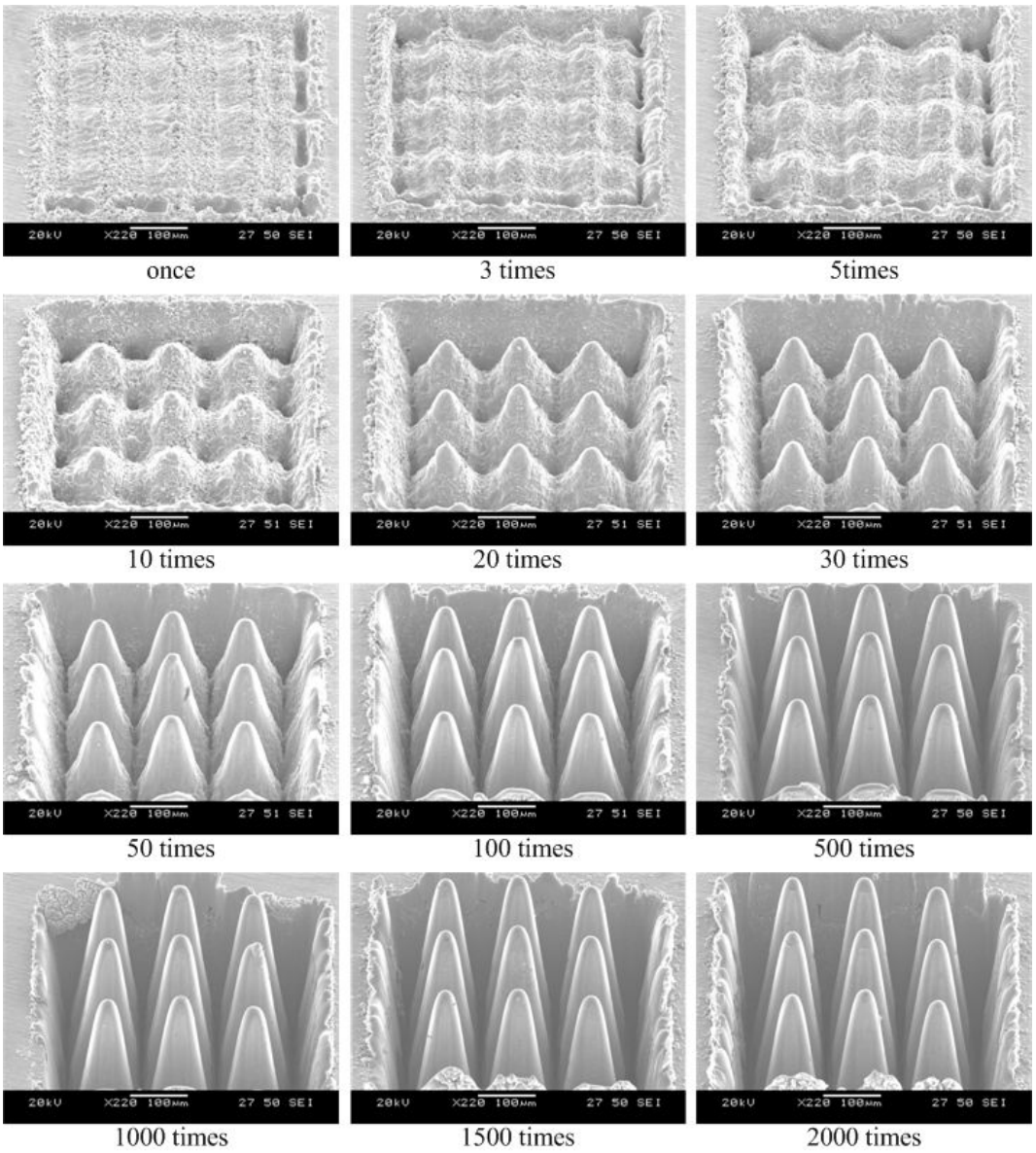

Figure 2.17 Recast layer piling procedure according to the scanning repeat count

2.4.6 Fabrication of micro-pin array on stainless steel

The micro-pin array was finally fabricated on stainless steel AISI 304, and figure 2.18 shows the result. A multi-line scanning path with 55 μm pitch was used, and the peak power density was 2.5 kW/mm^2. The scanning repeat count was 2000 times. The depth penetration was 441.9 μm, and the length of the piled recast layer was 159.1 μm. In addition, the final micro-pin length was 601.0 μm, the distance between the pin tips was 105 μm, and about 90 micro-pins could be fabricated per square millimeter.

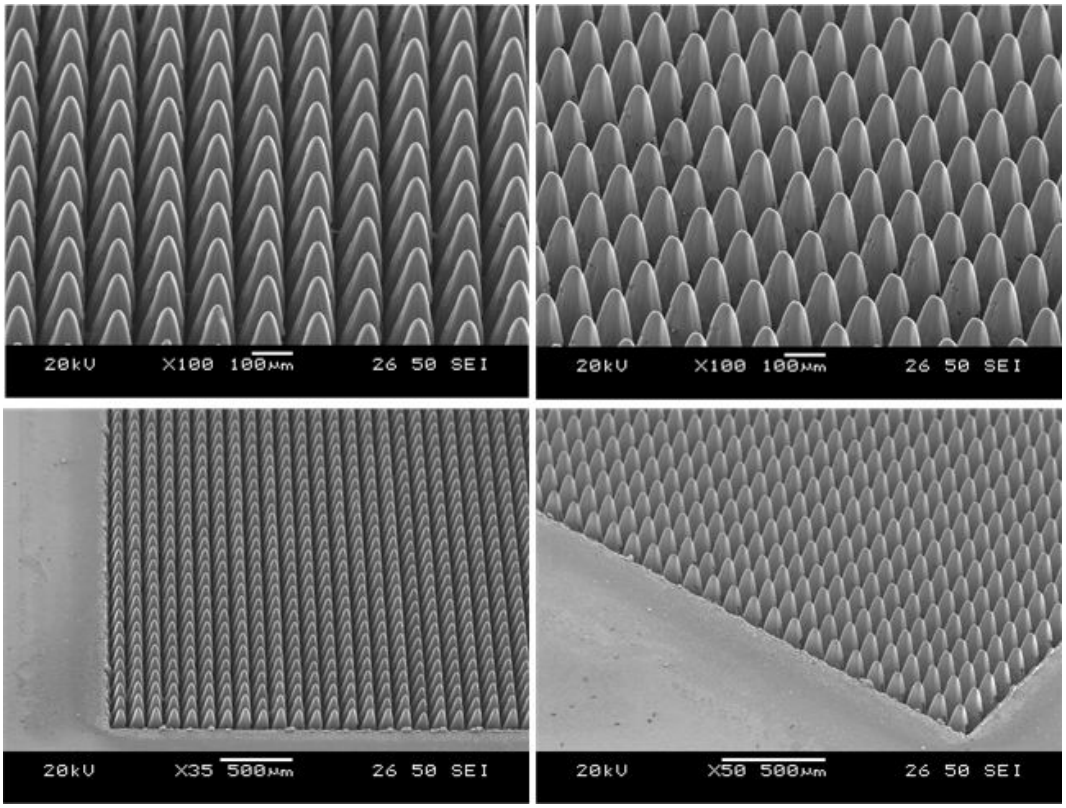

Figure 2.18 Micro-pin array fabricated on stainless steel AISI 304

Chapter 3

Fabrication of micro-pin array using laser beam machining and electrochemical etching

3.1 Laser beam machining of tungsten

Laser beam machining of tungsten is different with stainless steel. Tungsten is the metal that is hard to machine precisely. Melting point of tungsten is higher compared with stainless steel. Due to high melting point, high laser beam energy is needed to ablate tungsten [32]. Furthermore, thermal conductivity of tungsten is much high than stainless steel. Absorbed energy is transferred to the periphery rapidly because of high thermal conductivity. As a result, high laser beam energy is needed to machine tungsten and it makes precise machining hard.

Table 3.1 Thermal properties of tungsten and stainless steel AISI 304

	Tungsten	**AISI 304**
Thermal conductivity (W/m-K)	163.3	16.2
Melting point (°C)	3370	1400 – 1455

Machined surface of tungsten using laser beam machining is rough and has a lot of micro-cracks on recast layer. Therefore, in the case of precise machining using laser beam energy of tungsten, micro-cracks on recast layer should be removed by post process. Post processes to remove or inhibit recast layer generation have been researched. Typical post processes to remove recast layer are classified as mechanical, thermal, chemical or electrical processes [33]. In addition to these, several researches to remove or inhibit recast layer have been carried out, for example laser cleaning [34], thermal process[35] and under water process [36].

To fabricate micro-pin array on tungsten, electrochemical etching was selected as post process to remove recast layer in this research. A difference from general electrochemical etching post process is that bare metal as well as recast layer is machined in electrochemical etching process. Tungsten is the material that is hard to machine precisely using laser beam machining. For this reason, laser beam

machining process was used only for rough machining to fabricate pillar shape structure with blunt tip. In electrochemical etching process, pin shape structure was achieved as well as removal of recast layer. Sharp tip could be fabricated due to non-uniform current distribution in electrochemical etching [37, 38].

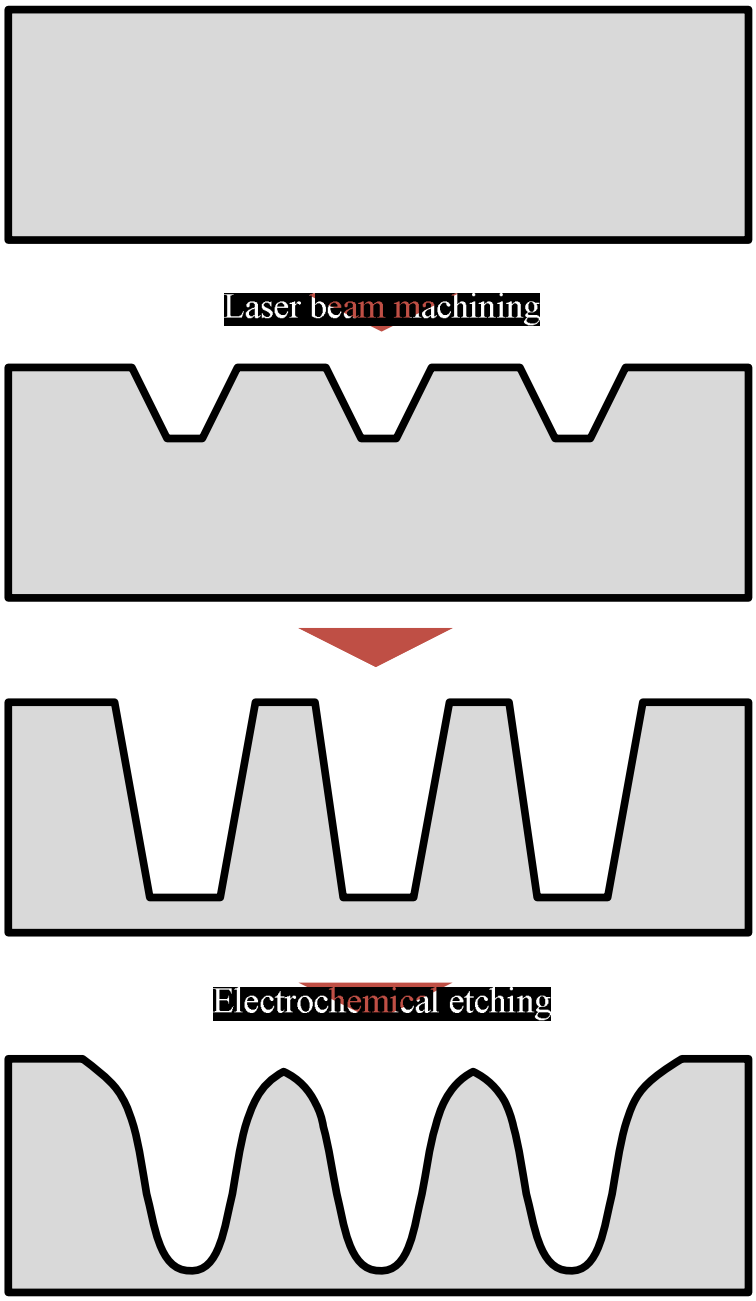

Figure 3.1 Procedure of laser beam machining and electrochemical etching

3.2 Asymmetric distribution of recast layer

Recast layer is the surface layer composed of redeposited metal that is created in thermal machining process like laser beam machining or electrical discharge machining. In laser beam machining, recast layer can form into a mass due to high laser beam energy. Moreover, there is molten metal pool on the machined area. In the molten metal pool, there are many forces like surface tension, gravity and photon pressure as shown in figure 3.2 [24]. By the action of these forces, molten metal forms a certain flow due to laser beam scanning and molten metal's fluidity [39].

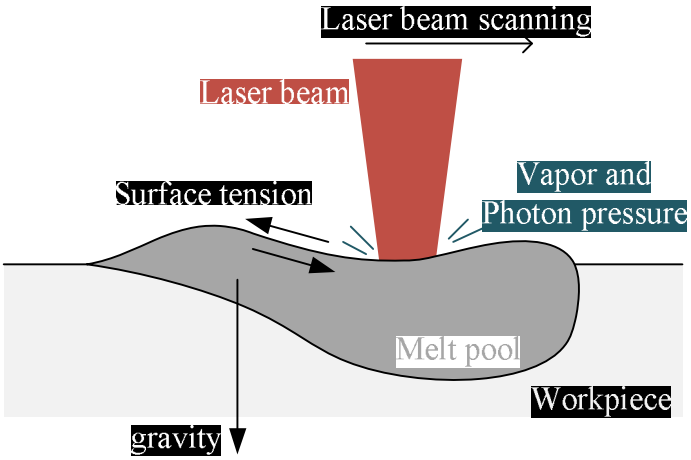

Figure 3.2 Forces in molten metal pool [24]

Asymmetric recast layer can be formed due to this molten metal flow and thermal property of tungsten. To fabricate micro-pin array using laser beam machining, repetitive and unidirectional laser beam scanning is performed and unidirectional molten metal flow is formed. In addition, molten metal solidify rapidly in the case of tungsten due to high thermal conductivity. As a result, asymmetric recast layer can be formed and it can cause non-uniform machining in electrochemical etching process.

To prevent asymmetric recast layer distribution, scanning sequence should be adjusted. Repetitive and unidirectional scanning sequence was changed to repetitive and bi-directional. In the condition that total scanning repetition number remained the same, scanning direction was changed in the opposite direction alternately as shown in figure 3.3 and 3.4. Using adjusted scanning sequence, recast layer was distributed uniformly.

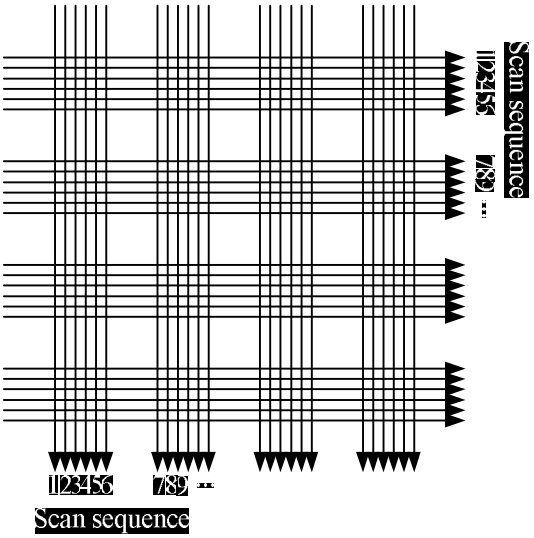

Figure 3.3 Unidirectional scanning sequence

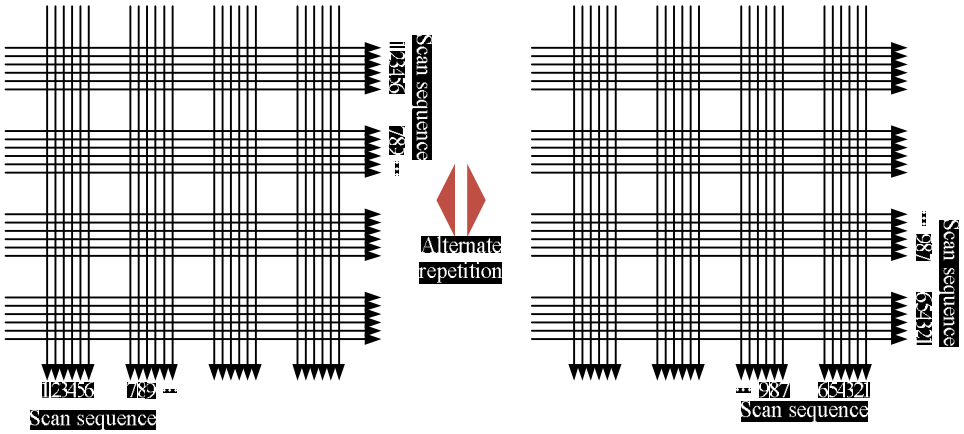

Figure 3.4 Bi-directional scanning sequence

3.3 System for laser beam machining and electrochemical etching

The equipment for laser beam machining was an ytterbium fiber laser (IPG photonics, YLP-C series) with a 1064 nm wavelength. The pulsed laser repetition rate can be controlled from 20 kHz to 80 kHz, and the pulse width is 100 ns. The laser beam power was between 6.0 W and 12.0 W. The laser beam scan speed of the galvanometer was fixed at 258.6 mm/s. The galvanometer scan head (SCANLAB AG, SCANcube 10) was equipped on a Z-axis stage to set optical focal length. The schematics of the laser beam machining system for rough machining are shown in figure 3.5.

After rough machining using laser beam machining, post process using electrochemical etching was carried out on the same stage. The schematics of electrochemical machining are shown in figure 3.6. Tool electrode, electrolyte circulation system (pool, tank, and pump) and pulse generator were equipped on laser beam machining system. For monitoring the experiment, oscilloscope and vision system were used additionally. Tungsten of 1.0 mm thickness was used as a workpiece. The workpiece was polished with sandpaper and cleaned in acetone using ultrasonic cleaner. Platinum sheet was used as tool electrode.

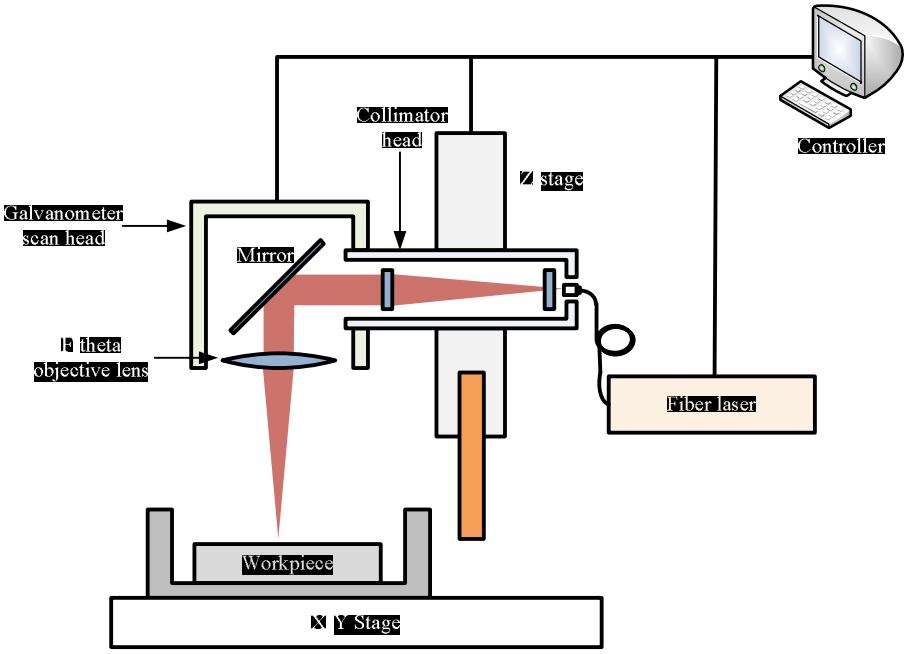

Figure 3.5 Experimental setup of laser beam machining for rough machining

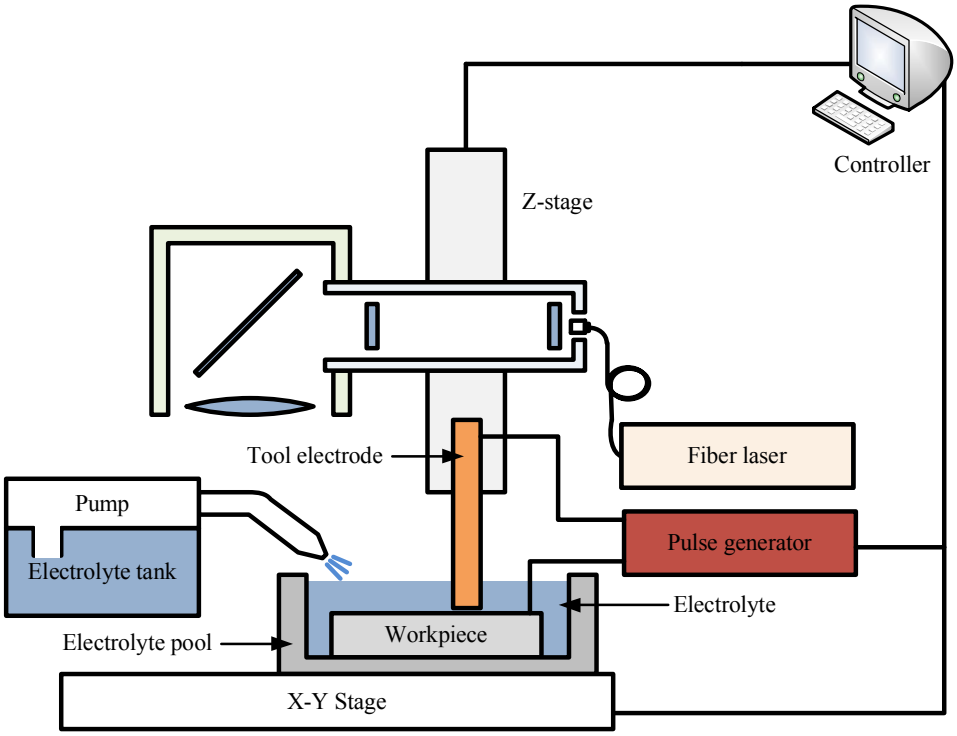

Figure 3.6 Experimental setup of electrochemical machining

3.4 Fabrication of micro-pin array on tungsten

To fabricate micro-pin array on tungsten, laser beam machining and electrochemical etching were carried out through as rough machining and post process. Machining conditions were indicated in table 3.2 and 3.3.

As a result, asymmetric distribution of recast layer occurred. Unidirectional and repetitive laser beam scanning indicated in figure 3.3 caused asymmetric distribution of recast layer. As shown in figure 3.7, recast layer was redeposited on one-side.

Table 3.2 Machining conditions of laser beam machining

Machining parameters	**Values**
Average power	8 W
Repetition rate	20 kHz
Scan speed	258.6 mm/s
Number of scanning repetition	2000 times

Table 3.3 Machining conditions of electrochemical machining

Machining parameters	**Values**
Electrolyte	NaOH solution
Electrolyte concentration	10 wt%
Applied voltage	10 V
Duty ratio	50% Pulse-on-time: 5 ms Pulse period: 10 ms
Machining time	30 seconds

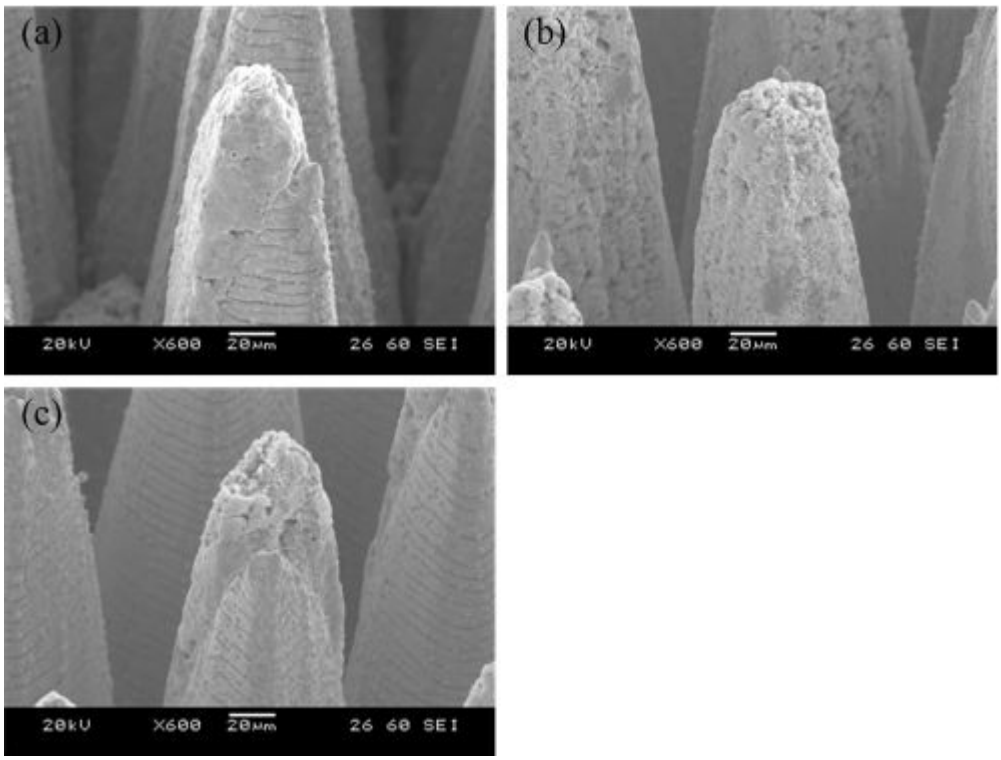

Figure 3.7 Asymmetric distribution of recast layer after laser beam machining of tungsten: (a) asymmetric distributed recast layer, (b) recast layer side and (c) the opposite side of recast layer

Furthermore asymmetric recast layer influenced electrochemical etching result. Electrochemical etching results were indicated in figure 3.8. Due to obstruction of recast layer, micro-pins were etched incompletely and asymmetrically. In figure 3.8a, redeposited material was not etched at all. When metal redeposition occurs, the metal can be oxidized. Bare metal was etched first because oxidized metal has different etch rate with bare metal. In figure 3.8b, micro-pin was sharpened but recast layer remained. Recast layer that is difficult to be machined using electrochemical etching influences micro-pin shape. Because recast layer plays a role as a protective layer and protects only one-side of bare metal, micro-pin shape becomes inclined as shown in figure 3.9c. To solve the aforementioned problems, the laser beam scanning sequence should be adjusted.

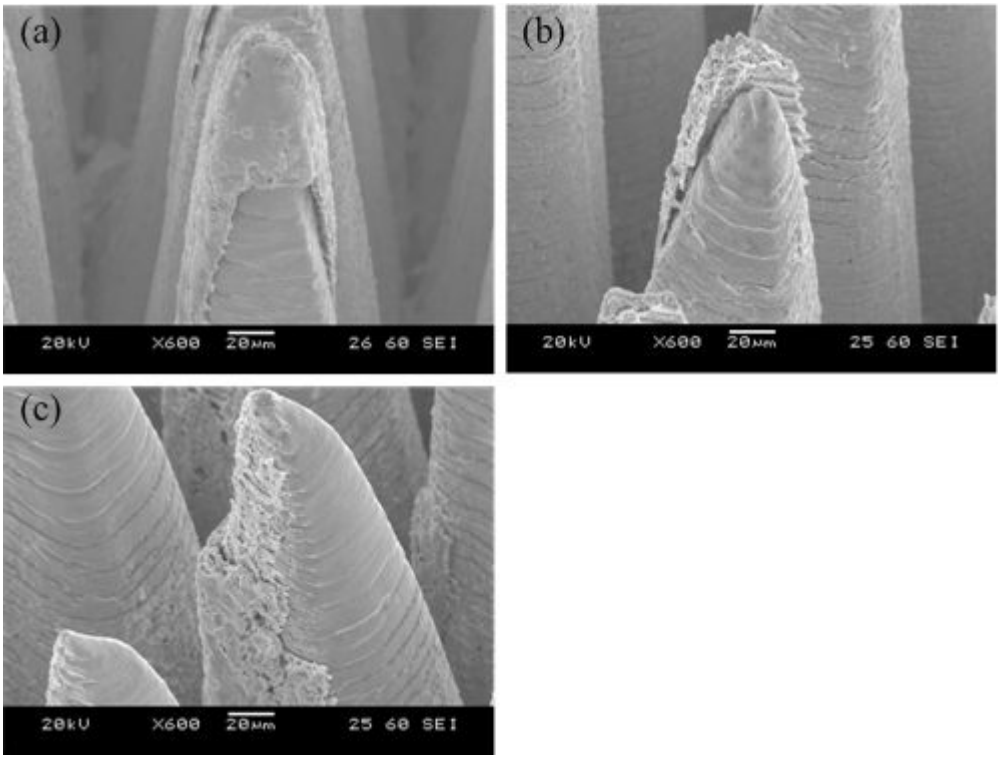

Figure 3.8 Electrochemical etched micro-pins with asymmetric recast layer: (a) remained recast layer after electrochemical etching process, (b) incomplete etched recast layer and (c) asymmetric etched micro-pin

3.4.1 Adjustment of laser beam scanning sequence

To etch micro-pins uniformly, adjustment of laser beam scanning sequence was applied in electrochemical etching process. The laser beam machining results that applied adjusted scanning sequence were presented in figure 3.9. There is no recast layer that redeposited in to a mass unlike figure 3.7. Micro-pin using adjusted laser beam scanning sequence had thin recast layer with micro-cracks.

Electrochemical etching results were also improved. Recast layer was removed completely and uniformly. Micro-pin tip was sharpened and the surface of micro-pin was fine.

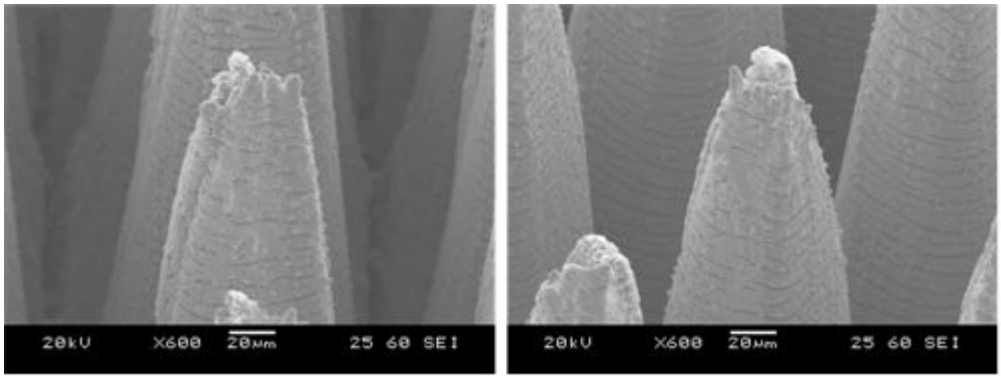

Figure 3.9 Micro-pin with uniform recast layer distributed

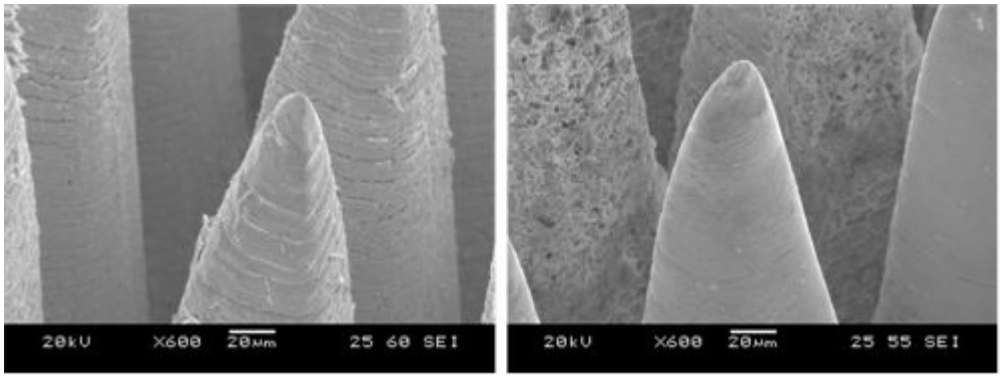

Figure 3.10 Electrochemically etched micro-pin using adjusted laser beam sequences

3.4.2 Machining characteristics in laser beam machining

Laser beam machining parameters were investigated for proper micro-pin shape and effective machining. Unlike machining parameter investigation in the laser beam machining of stainless steel, machining area and the volume of workpiece should be considered. Laser beam energy that is absorbed into tungsten spreads rapidly comparing with stainless steel because thermal conductivity of tungsten is much higher than stainless steel. Although all the machining conditions except machining area and the volume of workpiece were the same, machining results like pin shape, length and formation of recast layer were different as shown in figure 3.11. Thus laser beam machining parameter investigation results have meanings in experimental trend, not in absolute values.

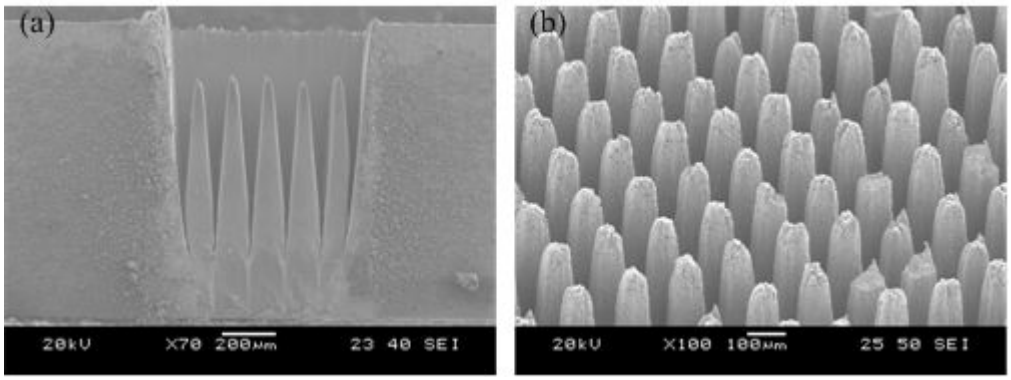

Figure 3.11 Micro-pin shapes of tungsten according to machining area and the volume of workpiece: (a) machining area of 0.575 mm x 0.575 mm on 3.0 mm x 3.0 mm x 1.0 mm workpiece, (b) machining area of 5.0 mm x 5.0 mm on 15.0 mm x 15.0 mm x 1.0 mm workpiece

Average power influenced micro-pin array shape and the results were represented in figure 3.12. Average power was adjusted as 6 W, 8W and 10 W. When the average power was too low, micro-pin array could not be fabricated completely as shown in figure 3.12a. Pin tip was too blunt to interlock on rough surface. Pin length was also too short. On the other hand, in the case of high average power, micro-pins were machined excessively. Micro-pin tip was sharpened because laser beam with high power influenced on apart of pin tip. However, high power laser beam also influenced on the top of the micro-pin. Micro-pin was shortened and it was not suitable for interlocking.

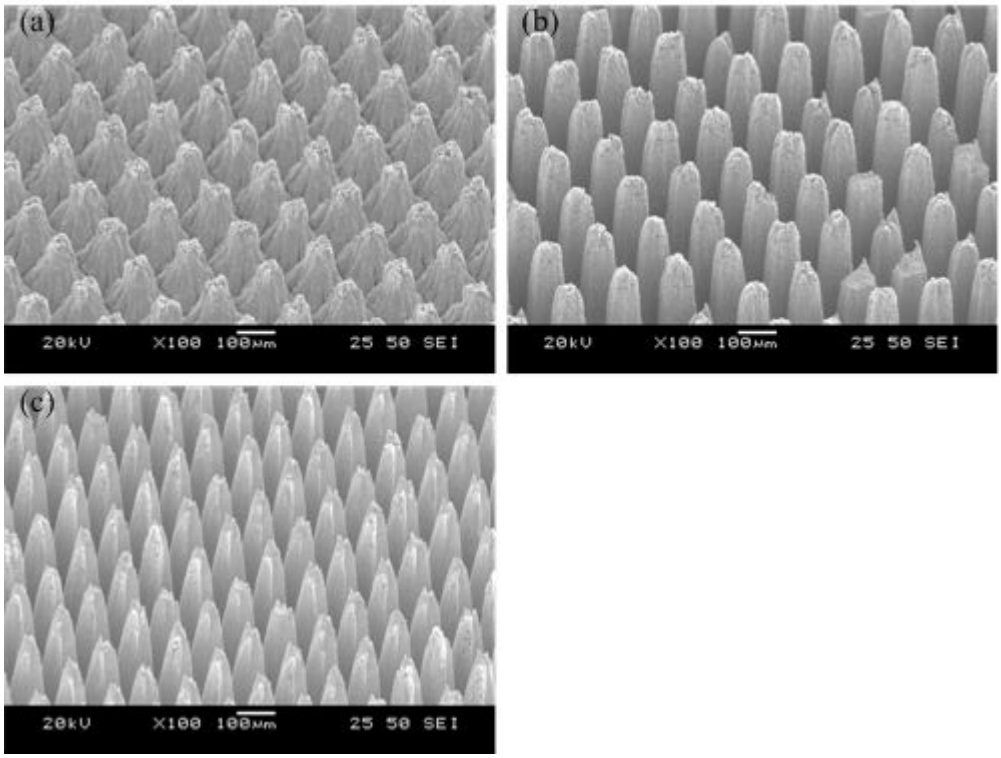

Figure 3.12 Micro-pin array according to average power of laser beam: (a) 6 W, (b) 8 W and (c) 10 W

To form the micro-pin with sharp tip as well as sufficient length, pitch of laser beam scanning path that was mentioned in figure 2.6 (chapter 2) was enlarged. Figure 3.13a is micro-pin array that machined under the same machining condition and scanning path with figure 3.12c. And its pitch in scanning path was 65 μm. The pitch of figure 3.13b and 3.13c were enlarged as 5 μm each. As shown in figure 3.13, length of micro-pins increased. But radius of micro-pins was blunt and the post process to sharpen micro-pin tip was needed. If it brings the same shape of micro-pins, small pitch is better than large pitch. Because more number of micro-pins can be fabricated using scanning path with small pitch.

As a result, micro-pin on tungsten cannot be machined into sharp shape using laser beam machining only. It could be machined into rough shape as shown in figure 3.12.b by laser beam of appropriate average power and it needs post process.

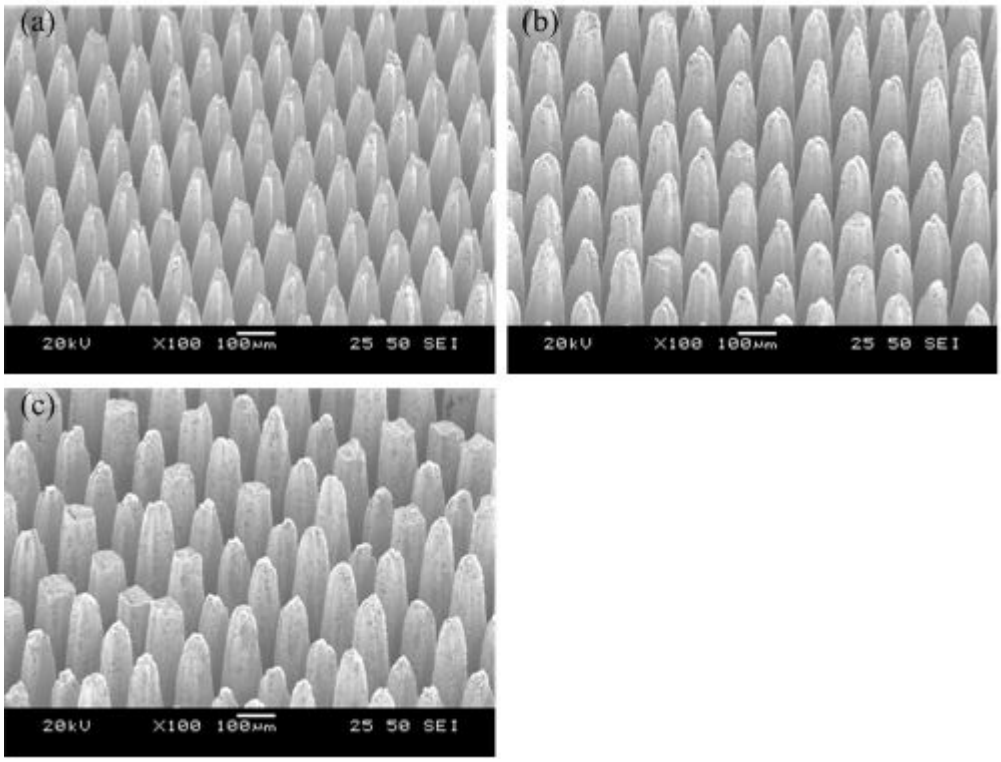

Figure 3.13 Micro-pin array according to laser beam scanning path: (a) 65 µm pitch, (b) 70 µm pitch and (c) 75 µm pitch

3.4.3 Machining characteristics in electrochemical etching

To fabricate micro-pin array with proper shape for interlocking, machining characteristics of electrochemical etching were also investigated. In electrochemical etching process of tungsten using sodium hydroxide (NaOH), electrochemical reaction is as follows.

$$W + 2NaOH + 6OH^- \rightarrow Na_2WO_4 + 4H_2O + 6e \quad \text{(Anode)}$$

$$6Na^+ + 6H_2O + 6e \rightarrow 6NaOH + 3H_2 \quad \text{(Cathode)}$$

$$W + 2NaOH + 2H_2O \rightarrow Na_2WO_4 + 3H_2$$

Machining condition that could etch only pin tip and maintain pin length should be selected. First, electrochemical etching using direct current was carried out. DC voltage has advantage over pulsed voltage in system simplification. Machined micro-pins were represented in figure 3.14 according to applied voltage. Machining time was 30 seconds. In the machining condition of 2 V and 5 V applied voltage, remained recast layer could be detected. On the contrary, in 8 V

applied voltage, it was machined excessively. As a result, micro-pin was fabricated bluntly. Electrochemical etching using direct current was too fast to fabricate sharp and fine tip.

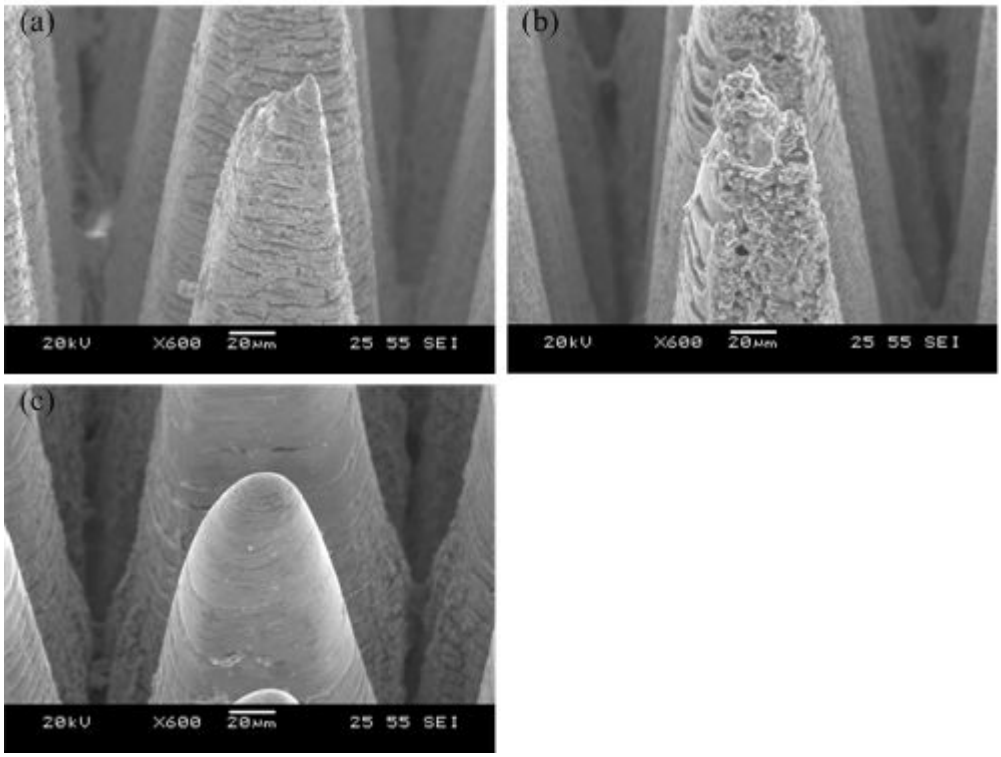

Figure 3.14 Micro-pin array according to applied voltage in electrochemical etching using direct current: (a) 2 V, (b) 5 V and (c) 8 V

Second, electrochemical etching using pulsed voltage was carried out. Though electrochemical etching using pulsed voltage needs complicated equipment like pulse generator, it enable more precise machining. Thus the machining condition for removing recast layer and sharpen pin tip could be found. Applied voltage was fixed as 10 V. Machining time and pulse ratio were controlled to fabricate proper shape of micro-pin array. As shown in figure 3.15a, recast layer was remained by machining conditions of 2.5 ms pulse-on-time, 10ms pulse period and 30 seconds machining time. On the contrary, pin tip became blunt in machining conditions of 1 ms pulse-on-time, 10 ms pulse period and 60 seconds machining time. Machining conditions of pulse-on-time 5 ms, pulse period 10 ms and machining time 30 seconds could fabricate micro-pin with sharp tip and sufficient length. In this condition, recast layer was removed completely and pin tip was sharpened.

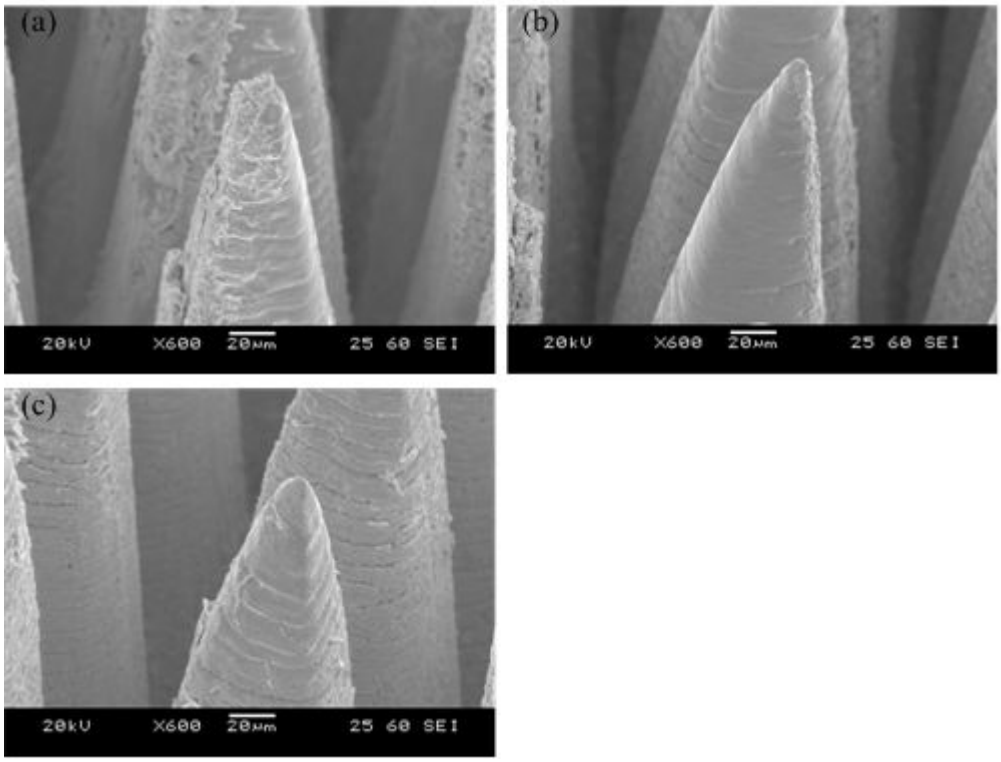

Figure 3.15 Micro-pin array according to machining time and pulse ratio in electrochemical etching using pulsed voltage: (a) pulse-on-time 2.5 ms, pulse period 10 ms, machining time 30 seconds, (b) pulse-on-time 5 ms, pulse period 10 ms, machining time 30 seconds and (c) pulse-on-time 1 ms, pulse period 10 ms, machining time 60 seconds

3.4.4 Fabrication of micro-pin array on tungsten

The micro-pin array was finally fabricated on tungsten, and figure 3.16 shows the result. Laser beam machining was used for rough machining. Average power was 8.0 W. Laser beam pulse repetition rate was 20 kHz and scan speed was 258.6 mm/s. The scanning repeat count was 2000 times. Electrochemical etching was used as post process. Electrolyte was 10 wt% NaOH solution. Pulsed voltage of 50% duty ratio was applied. Pulse-on-times was 5 ms and pulse period was 10 ms. Machining time was 30 seconds.

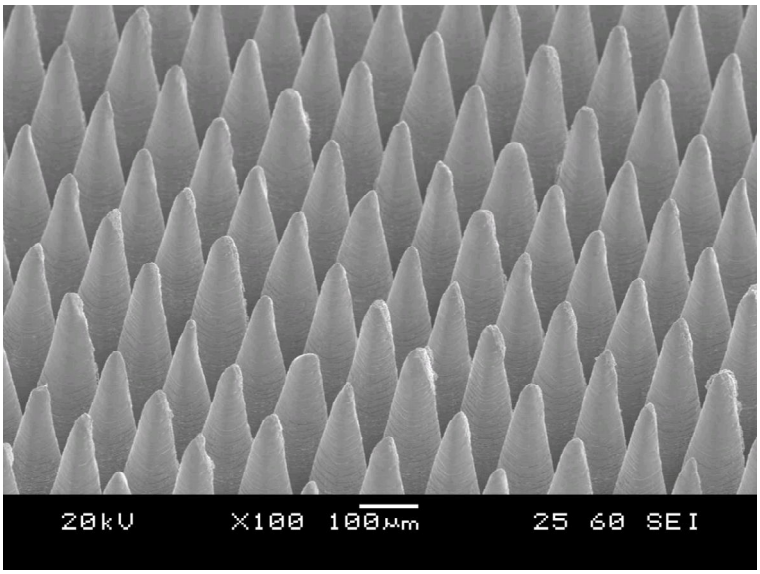

Figure 3.16 Micro-pin array fabricated on tungsten

Chapter 4

Interlocking of micro-pin array on rough surface

4.1 Interlocking on rough surface

Micro-pin array that was fabricated on metal can be used for interlocking on rough surface. It can also attach on vertical rough surface using interlocking force. Sharp tip of micro-pin array can interlock with the irregularities on the rough surface.

There were some researches about attachment to vertical surface using interlocking. Spiny-bot could attach to vertical rough wall like concrete using spine engagement [10]. It used sharp hook-shape needle and foot using compliant mechanism. In nature, some insects use interlocking [16]. Friction force between rough surface and the claws of insects was studied. In the study, comparison of the claw tip dimensions with the surface texture was carried out.

In this research, attaching to vertical surface using interlocking force of micro-pin array was performed successfully as shown in figure 4.1. Target vertical surface was aluminum that was machined by EDM (electrical discharge machining) and its surface roughness was Ra 3.138 μm. Micro-pin array was fabricated on 15 mm x 15 mm x 3 mm stainless steel plate. It could load 46.3 g including self-weight of micro-pin array.

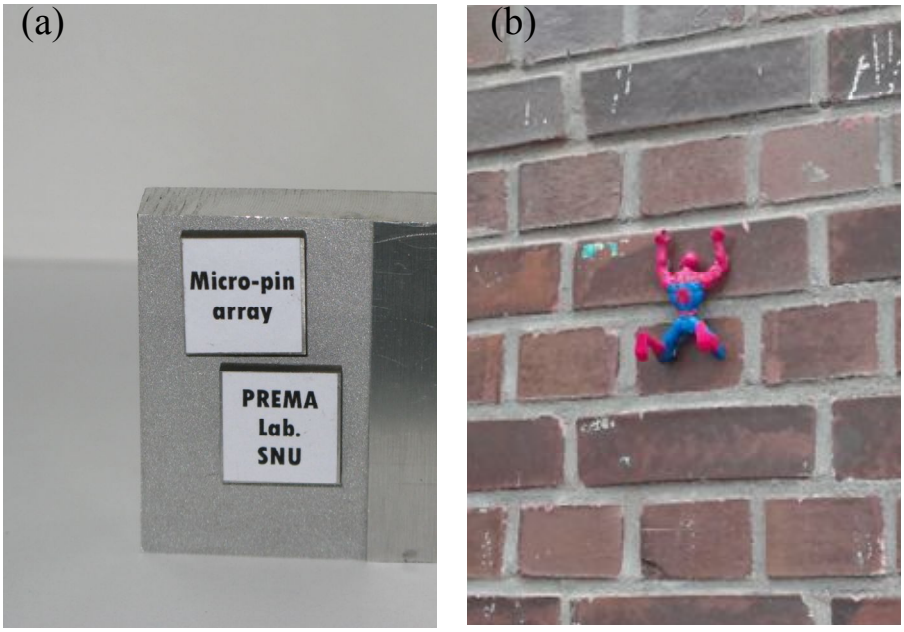

Figure 4.1 (a) Micro-pin array attached to vertical rough surface using interlocking force, (b) demonstration of interlocking using toy figure

To confirm quantitative properties, interlocking force measurement system was set up using load cell and linear stage. As shown in figure 5.2a, the probe installed to load cell pushed the micro-pin array on rough surface. At this process, to exclude momentum caused by the shape of workpiece that micro-pin array was fabricated, the horizontal direction forces that micro-pin array was able to endure in laid condition were measured. For above-mentioned reasons that exclude momentum, micro-pin was fabricated on thin plate with 0.5 mm thickness. Fabricated area of micro-pin array was 3 mm x 3 mm. Contact point of probe was on the center of the pin length, not on base. It was presented in figure 5.2b.

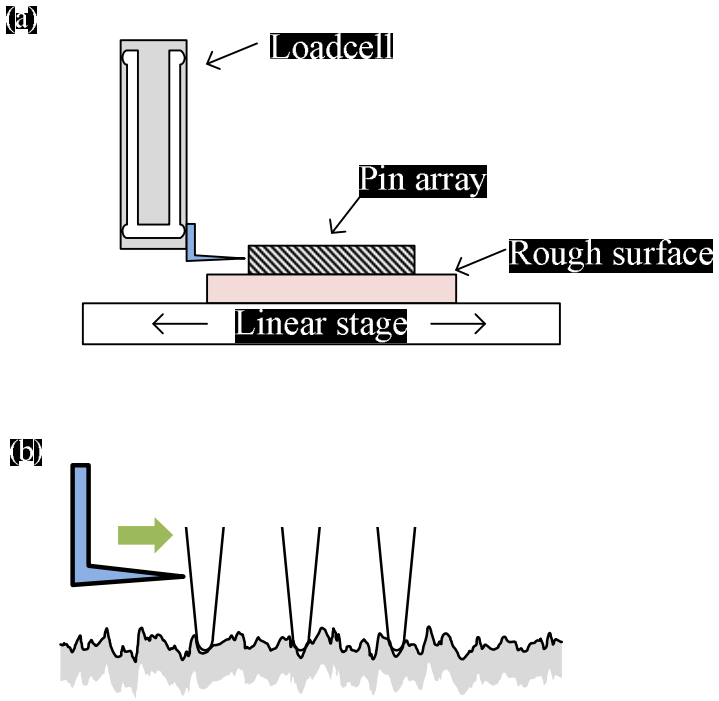

Figure 4.2 (a) Interlocking force measurement system and (b) enlarged diagram of the probe's contact point

Interlocking force was measured. It could generate 696 mg/mm^2 and it was 10 times more than normal surface without micro-pin array. Normal surface without micro-pin array showed just friction force, 0.069 mg/mm^2.

Interlocking forces according to micro-pin density were measured. Results are indicated in figure 4.3. As a result, interlocking force was proportionate to micro-pin density. The more micro-pin was fabricated, the more interlock occurred. It means that interlocking of micro-pin array and surface irregularities is probability event.

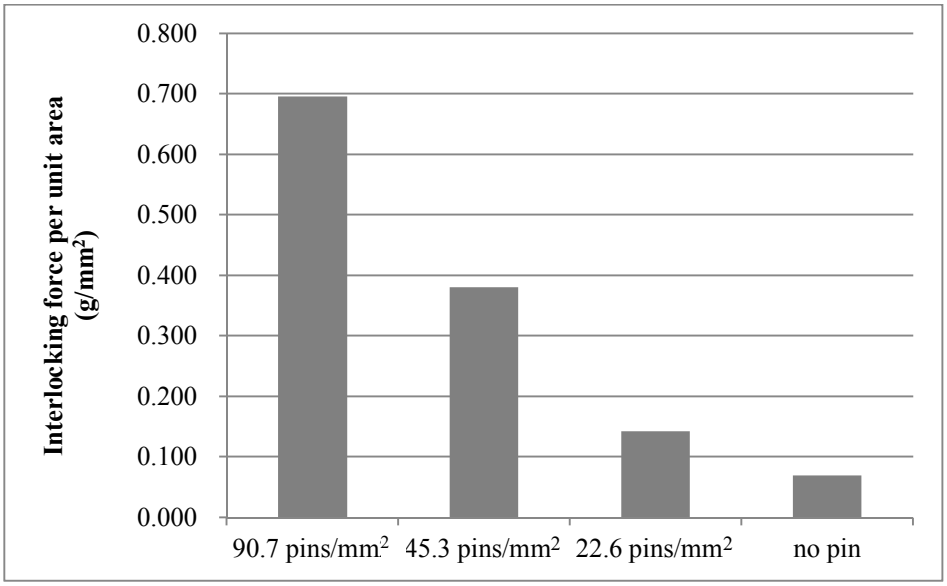

Figure 4.3 Interlocking force per unit area according to micro-pin density

Interlocking forces according to target surface properties were also measured. Target surface materials were machined aluminum and sandpaper. In the case of aluminum, machining condition was controlled to make surface with various surface profiles. In the case of sand paper, several kinds of grit number were used for various surface profiles.

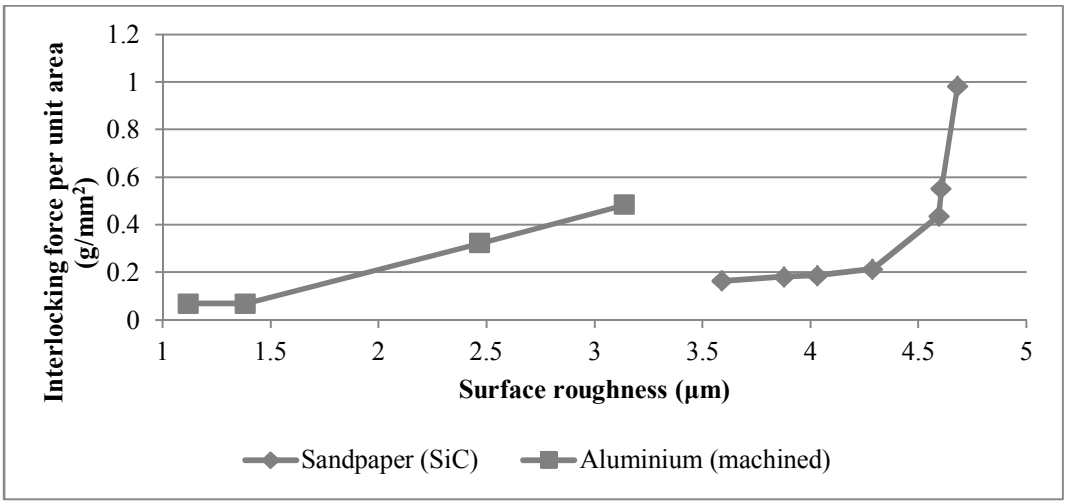

Figure 4.4 Interlocking force per unit area according to target surface properties (material and surface toughness)

The results were represented in figure 4.4. The more interlocking force was generated on rougher surface. It means larger irregularities on surface generate more force when it interlocks with micro-pins. On the other hand, some aluminum surface generated more force than sandpaper surface, in spite of low surface roughness. Since friction coefficient between stainless steel and aluminum (0.85) is higher than friction coefficient between stainless steel and SiC (0.81), it could generate more interlocking force.

Measurements of interlocking forces according to normal load were also carried out. In this measurement, interlocking force and normal load were in proportionate relationship.

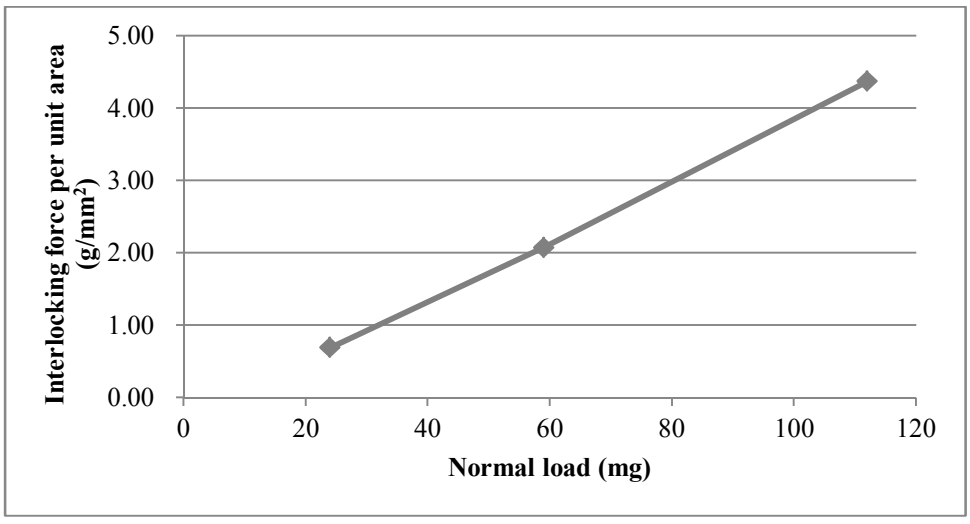

Figure 4.5 Interlocking force per unit area according to normal load

4.2 Principle of the micro-pin array interlocking on rough surface

Interlocking properties of micro-pin array was studied in previous part. In this part, quantitative analysis was carried out by pin-surface interlocking modeling and its verification. Previous researches about interlocking have limitation. Probability simulation about spine-surface modeling was carried out [10]. But this research have limitation that no verification about proposed model. On the other hand, measurement of the force that generated in insect's claw was performed using load cell [16]. However, there was no analysis about measurement result. In previous research about interlocking, there was no verification of experimental results and model. In this research, interlocking force measurement and modeling were carried out. Interlocking modeling was established and verification of the model was carried out by comparison between modeling result and actual force measurement. At last, interlocking force estimation based on the established model was carried out using surface profile investigation.

4.2.1 Pin-surface interlocking modeling

To establish the pin-surface interlocking model, the contact point was

simplified. In simplified model, the contact point can be regarded as the incline. Then, the pin-surface interlocking can be converted friction model on the inclined plane. In this model, inclined angle is contact angle between surface irregularity and micro-pin tip.

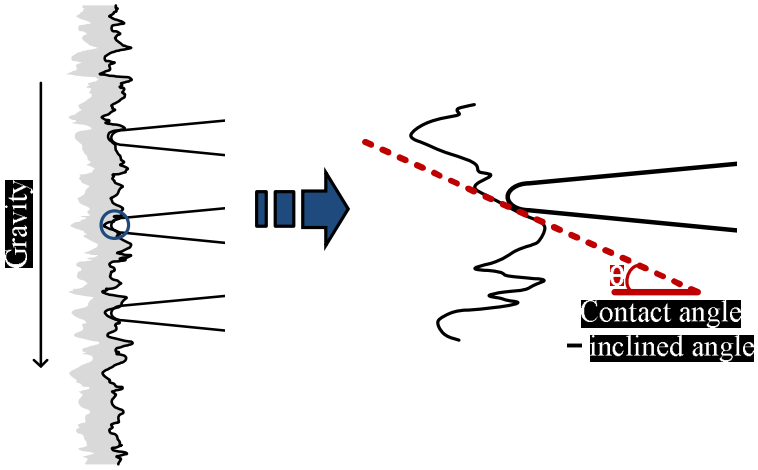

Figure 4.6 Interlocking model that simplified as friction in the incline

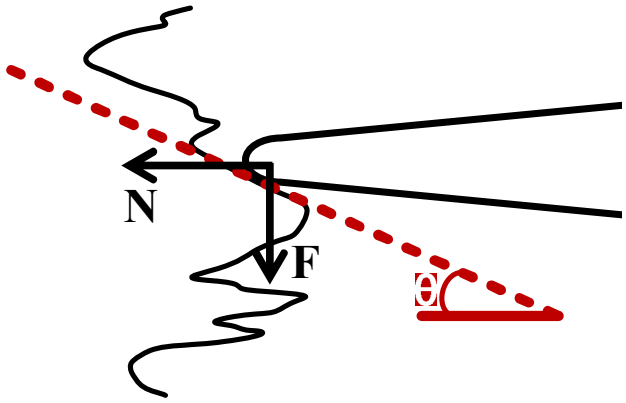

Figure 4.7 Forces acting on contact point

Forces acting on contact point can be represented like figure 4.7. And the friction force on contact point is as follows.

$$\mu(\mathrm{F}\cdot\cos\theta + N\cdot\sin\theta) = F\cdot\sin\theta - N\cdot\cos\theta$$

It can be arranged as follows.

$$\mathrm{F} = \mathrm{N}\frac{1+\mu\cdot\cos\theta}{\tan\theta-\mu}$$

F is generated interlocking force, μ is friction coefficient, N is normal force to the surface and θ is contact angle. It can be expressed as graph in figure 4.8. In this graph, infinite F means that friction force is always larger than sliding force due to low inclined angle.

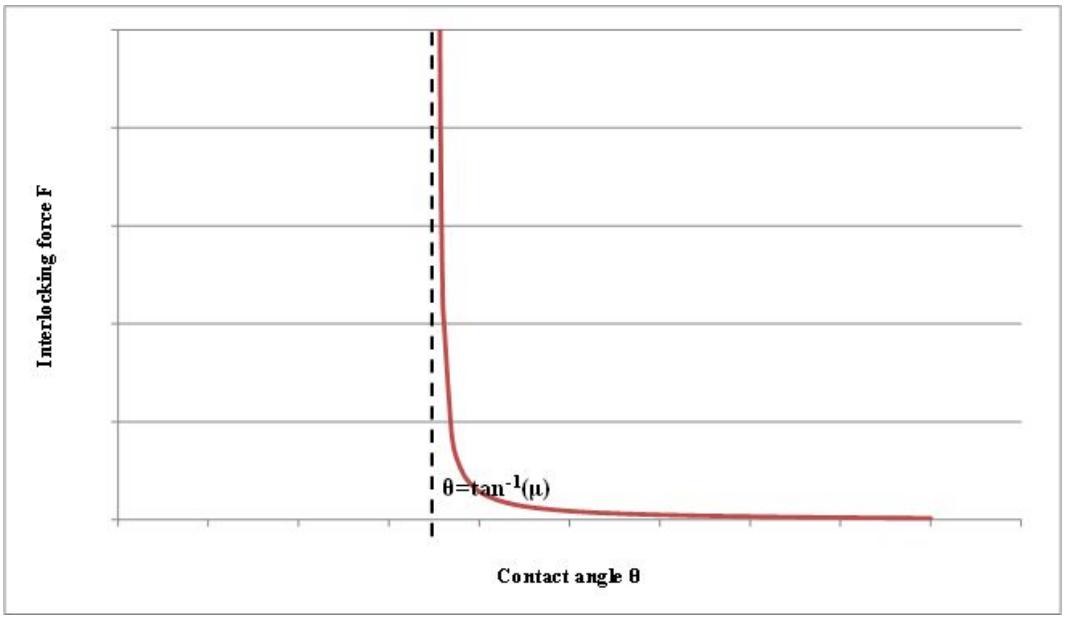

Figure 4.8 Interlocking force F relative to contact angle

To verify established model, target surface was artificially modified to control the contact angle using laser beam machining. Examples of modified surface were shown in figure 4.9. Using laser beam machining, grooves of various shape were fabricated. The depth and slope of groove can be shaped intentionally by controlling machining parameters. As a result, the contact angle of interlocking can be also controlled. In addition, space between grooves was the same with space between micro-pins. Since grooves and micro-pins were arranged with the same space, all micro-pins could be regarded to interlock with the groove. In other word, it enables to ignore the probability of interlocking.

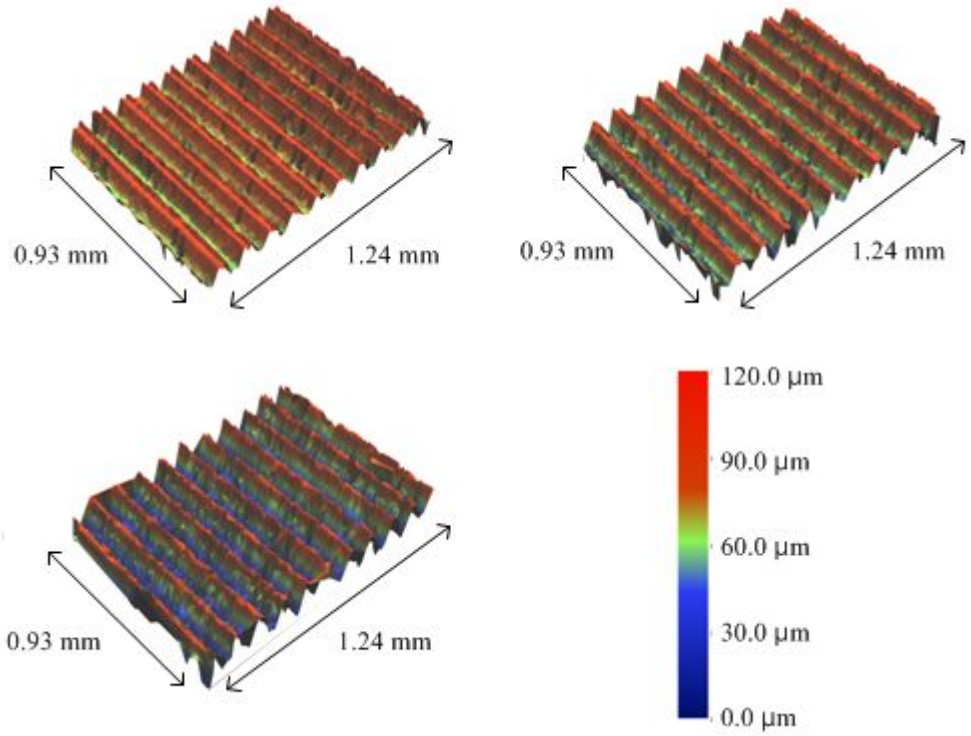

Figure 4.9 Modified surfaces. Groove shape can be controlled and probability of interlocking can be ignored.

As a result, interlocking forces on modified surface were measured and compared with the forces calculated from established model. It was shown in figure 4.10. Friction coefficient was 0.71 (stainless steel – stainless steel). It can be observed that measured force followed the calculated force. After all, established model was verified by comparing measured actual force and calculated force.

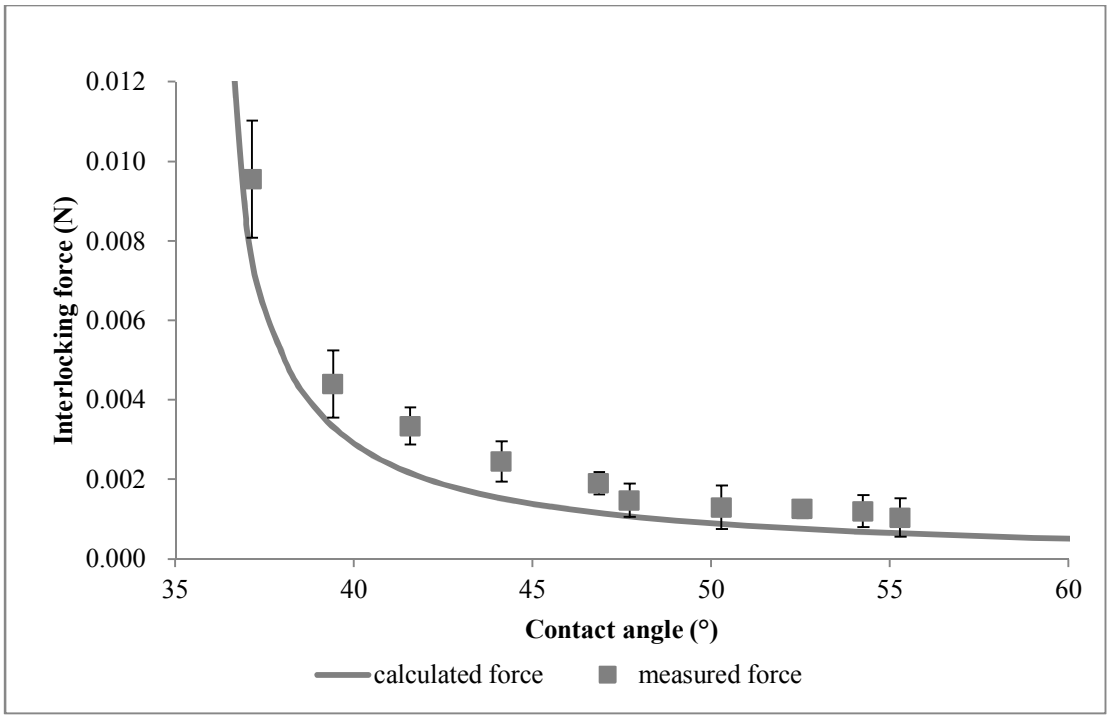

Figure 4.10 Verification of model by comparing measured actual force and calculated force

4.2.2 Interlocking force estimation on a rough surface

Based on the modeling result, interlocking force in a surface can be estimated. The slope angle at each point on a surface can be calculated by surface profile investigation. And interlocking force can be estimated on a surface by extracting meaningful slope angle.

On a surface, there are many points not to participate in interlocking. Moreover, there are the points that generate little interlocking force. Thus, meaningful slope angle should be extracted for accurate estimation.

First, the points that generate little interlocking force should be excepted from meaningful slope angle. As shown in figure 4.11, flatness and peak points are exceptions. Contact angle of flatness point is too high to generate interlocking force. Peak point is also hard to interlock with micro-pin array.

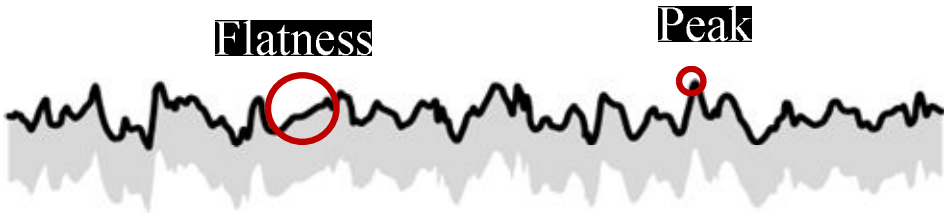

Figure 4.11 The points that is hard to generate interlocking force

Second, bending of micro-pin should be considered. Since micro-pin array cannot cover the entire surface, a pin's effective area should be calculated. In this process, bending deformation and extracted slope angle affect each other. Therefore, iteration is needed until convergence of calculated value. Surface profile investigation and force measurement were carried out on sandpaper and aluminum. Estimation results were shown in figure 4.12. Estimated values followed the tendency, but they were larger than measured force. Larger values were resulted, because slope angle used in force calculation was extracted angle that generate large force.

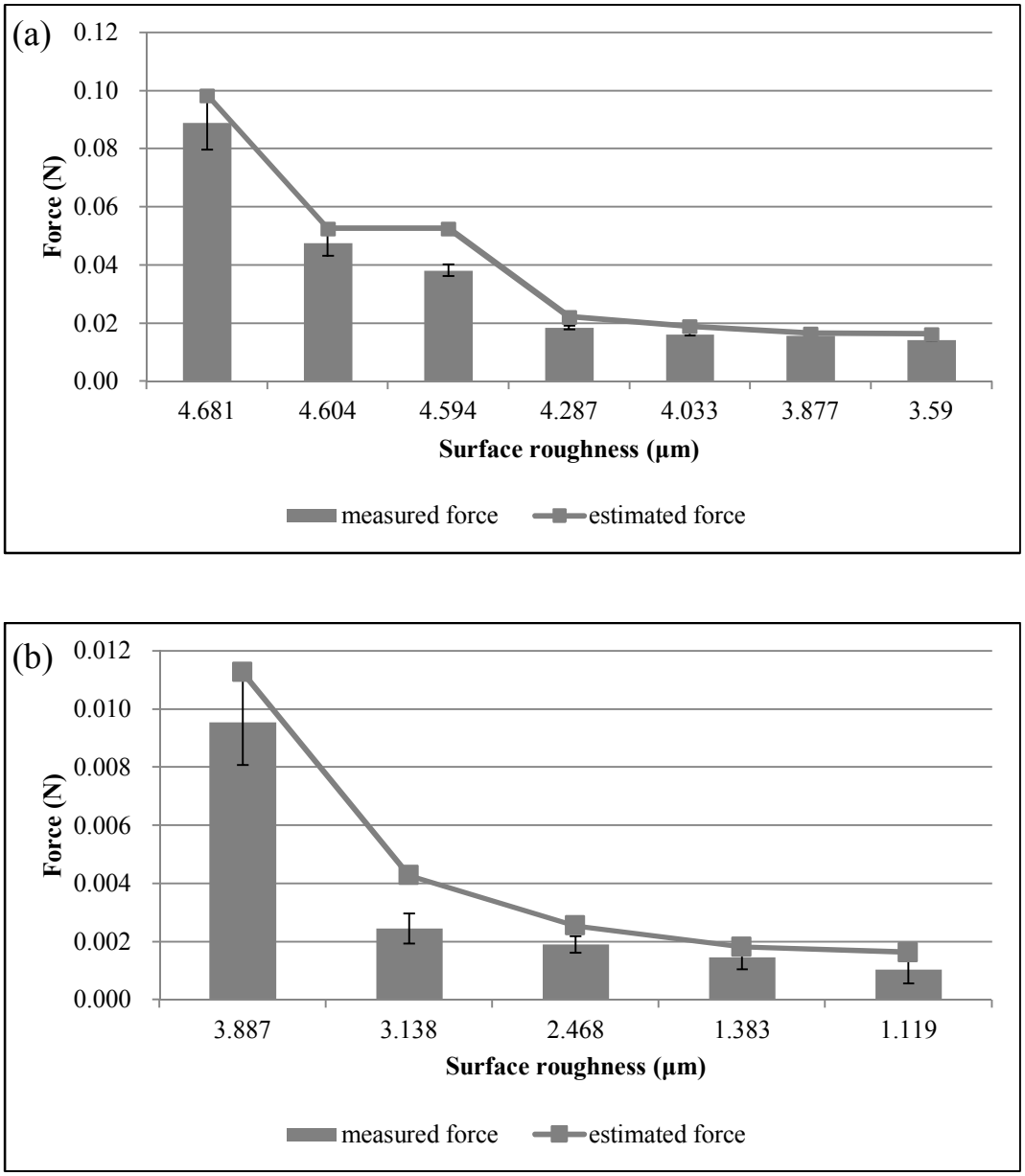

Figure 4.12 Verification of interlocking force estimation by comparing measured actual force and estimated force: (a) on sandpaper and (b) on aluminum

4.3 Interlocking force according to micro-pin shape

As shown in above results, interlocking force is determined by contact point between micro-pin tip and rough surface. The contact point conditions are changed by micro-pin shape. Moreover, micro-pin shape can be controlled by machining condition in fabrication process. In this part, interlocking force measurements according to micro-pin shape and machining conditions in chapter 2.4 were carried out. The micro-pin arrays that used in this measurement is fabricated in chapter 2.4.

In table 4.1, interlocking forces according to laser beam scanning path were represented. Pin density of single line scanning path is much higher than multi-line scanning path. Pin length and tip radius were superior in multi-line scanning path. This result signified that pin length and tip radius have stronger influence on interlocking force than pin density. Table 4.2, table 4.3 and table 4.4 each show interlocking forces according to line space, laser beam power density and laser beam scan speed. All the results represent that micro-pin shape of long pin length and small pin tip radius is at an advantage for high interlocking force.

Table 4.1 Interlocking forces according to laser beam scanning path

Laser beam scanning path	**Single line**	**Multi-line**
Pin density	330.6 pins/mm^2	90.7 pins/mm^2
Pin length	313.2 μm	601.0 μm
Pin tip radius	14.0 μm	9.2 μm
Interlocking force	0.107 g/mm^2	0.696 g/mm^2

Table 4.2 Interlocking forces according to line space

Line space	**46 μm**	**55 μm**	**65 μm**
Pin length	449.0 μm	601.0 μm	565.5 μm
Pin tip radius	14.1 μm	9.2 μm	23.6 μm
Interlocking force	0.527 g/mm^2	0.696 g/mm^2	0.392 g/mm^2

Table 4.3 Interlocking forces according to laser beam power density

Laser beam power density	**1.00 kW/mm^2**	**1.75 kW/mm^2**	**2.50 kW/mm^2**	**3.25 kW/mm^2**
Pin length	265.7 μm	493.0 μm	601.0 μm	582.1 μm
Pin tip radius	13.7 μm	10.1 μm	9.2 μm	9.8 μm
Interlocking force	0.141 g/mm^2	0.528 g/mm^2	0.696 g/mm^2	0.655 g/mm^2

Table 4.4 Interlocking forces according to laser beam scan speed

Laser beam scan speed	**158.6 mm/s**	**258.6 mm/s**	**358.6 mm/s**	**408.6 mm/s**
Pin length	514.2 μm	601.0 μm	514.1 μm	474.2 μm
Pin tip radius	13.6 μm	9.2 μm	13.2 μm	13.2 μm
Interlocking force	0.235 g/mm^2	0.696 g/mm^2	0.488 g/mm^2	0.460 g/mm^2

Chapter 5

Applications of micro-pin array

5.1 Fabrication and application of tilted micro-pin array

Tilted micro-pin array was fabricated on stainless steel. Tilted micro-pin array can generate more interlocking force, while the direction of interlocking force is limited to one-way. It can generate more interlocking force because the dispersion of interlocking force was occurred by tilted micro-pin array.

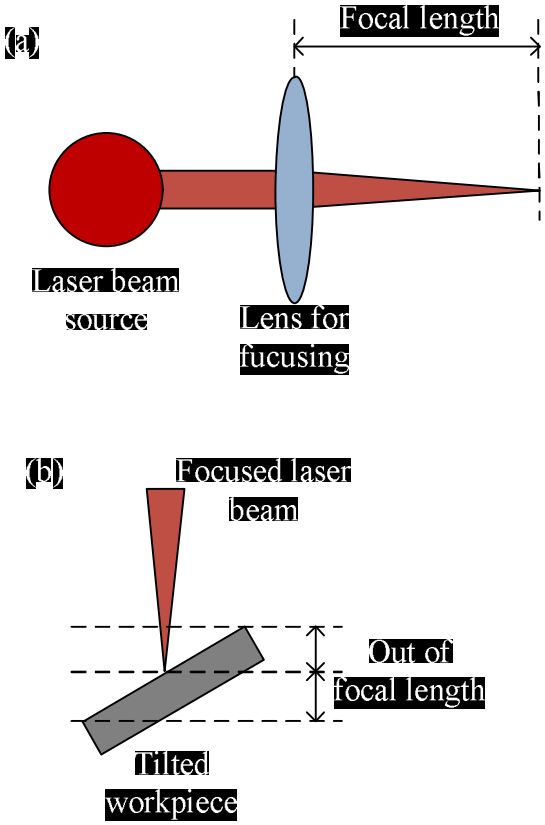

Figure 5.1 (a) focal length of laser beam machining, (b) problems in laser beam machining of tilted workpiece

To fabricate tilted micro-pin array, laser beam machining was carried out on tilted workpiece. Focal length of laser beam should be considered in this process. To machine something with laser beam energy, laser beam from laser beam source should be focused on a point. When laser beam is focused, focal length of laser beam was defined by wavelength of laser beam. Machining efficiency of laser beam is decreased on the area that strayed out of focal length. In the case of tilted workpiece, outer part of machining area is strayed out of focal length and this causes some problems. As shown in figure 5.2a, micro-pin array with different length was fabricated. The more it gets out of the focal length, the more machining efficiency decrease occurs. Moreover, micro-pin array lost its shape and collapsed as shown in figure 5.2b.

To resolve problems of focal length, z-axis stage which was equipped galvanometer scan head moved in sync with scanning speed. As a result, tilted micro-pin arrays with several degrees could be fabricated as shown in figure 5.3.

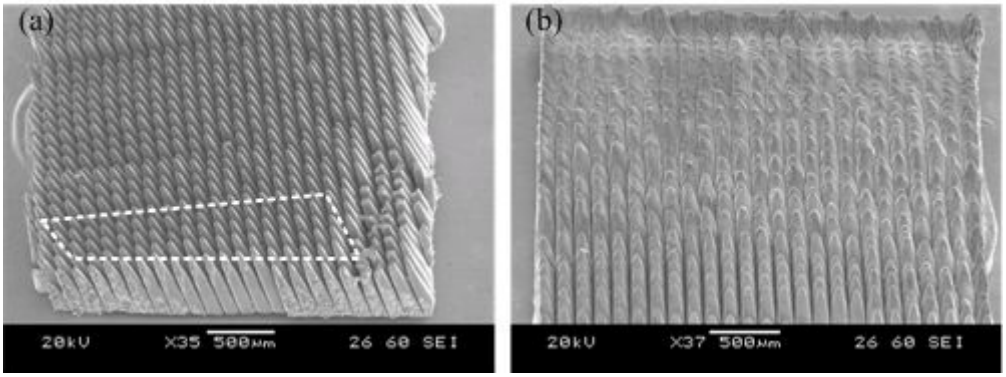

Figure 5.2 Machining problems that were caused by focal length: (a) different pin length, (b) non-uniform shape of micro-pin array

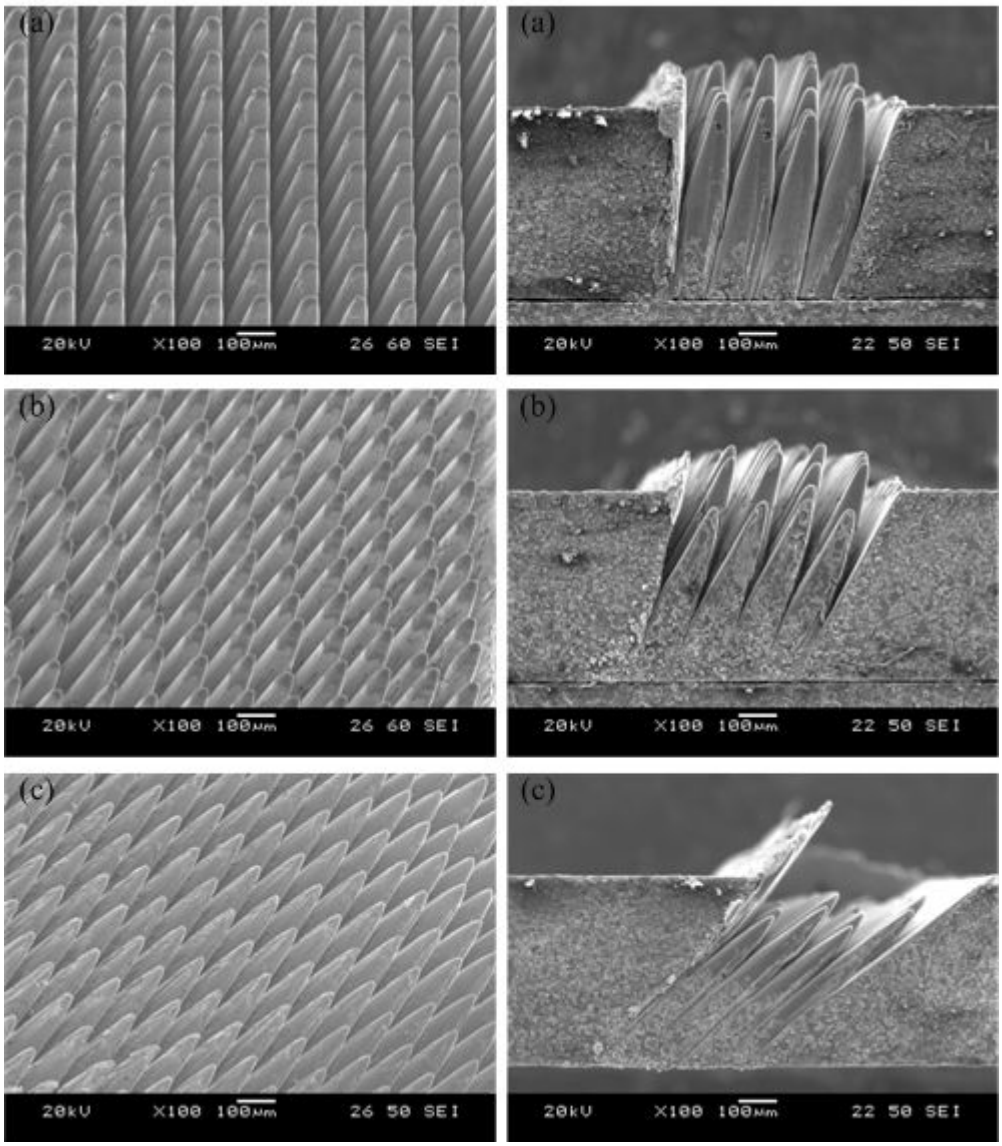

Figure 5.3 Tilted micro-pin array: (a) 10 degrees, (b) 20 degrees and (c) 45 degrees

Moreover, interlocking forces of tilted micro-pin arrays were measured on rough surface (sandpaper). To verify both directivity and magnitude of interlocking force, measurements were carried out bi-directionally. Measurement results were represented in figure 5.4. Tilted micro-pin array generated more interlocking force. However, it generated little force in the opposite direction. Under -20 degrees, tilted micro-pin array could not generate interlocking force. Thus, tilted micro-pin array can be used in the condition which the direction of required force is fixed as one-direction.

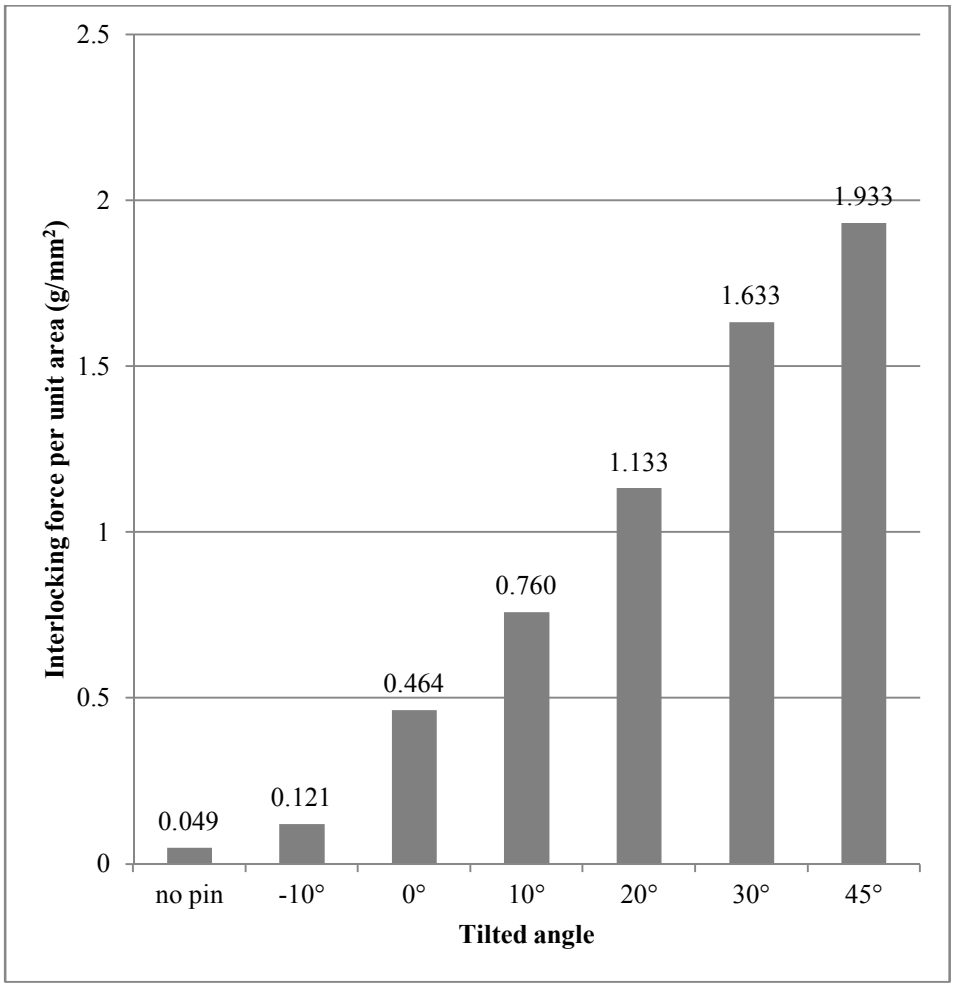

Figure 5.4 Interlocking forces of tilted micro-pin arrays

5.2 Fabrication and application of flexible base micro-pin array

In interlocking of micro-pin array on rough surface, the number of micro-pins that participate in interlocking is important factor. The number of micro-pins that participate in interlocking is proportional to contact area of whole micro-pin array. However, contact area of micro-pin array decreases extremely on curved surface or the surface with waviness. Micro-pin array with flexible base was fabricated to keep the contact with curved surface. Micro-pin array with flexible base can be deformed adaptively and keep large contact area unlike micro-pin array with rigid base as shown in figure 5.5.

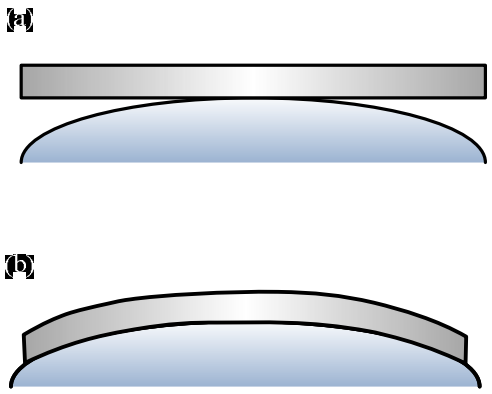

Figure 5.5 (a) small contact area of rigid base micro-pin array, (b) adaptive deformation and large contact area of flexible base micro-pin array

To fabricate micro-pin array with flexible base, stainless steel was used as micro-pins and polydimethylsiloxane (PDMS) was used as flexible base. Whole procedure for fabricating micro-pin array with flexible base is represented in figure 5.6. In the process of fabrication of metal micro-pin array, laser beam machining using recast layer piling was applied. Next, the surface of micro-pin was coated by thermoplastic resin (paraffin wax). Thermoplastic resin played 2 roles. The first role is protective layer from electrochemical etching and the second role is fixing micro-pins without base until PDMS forming. Metal base of micro-pin array was eliminated by electrochemical etching. Sulfuric acid aqueous was used as electrolyte and direct current was supplied. Concentration of sulfuric acid was 0.5 M and applied voltage was 5 V DC. Because micro-pin can be lost by violent bubble generation, more voltage cannot be applied.

In electrochemical etching process, only metal base was machined except micro-pins. The surface of micro-pin was protected by thermoplastic resin. In the case of base side, metal base was etched first. Since it was electrically separated, no more electrochemical etching occurred, when metal base was etched completely and the bottom part of micro-pin was exposed. After elimination of metal base, base was displaced by PDMS and thermoplastic resin was removed. For removing resin, micro-pin array with resin was cleaned in 90 degree Celsius water of ultrasonic vibrating cleaner. As shown in figure 5.7. flexible base micro-

pin array was fabricated successfully.

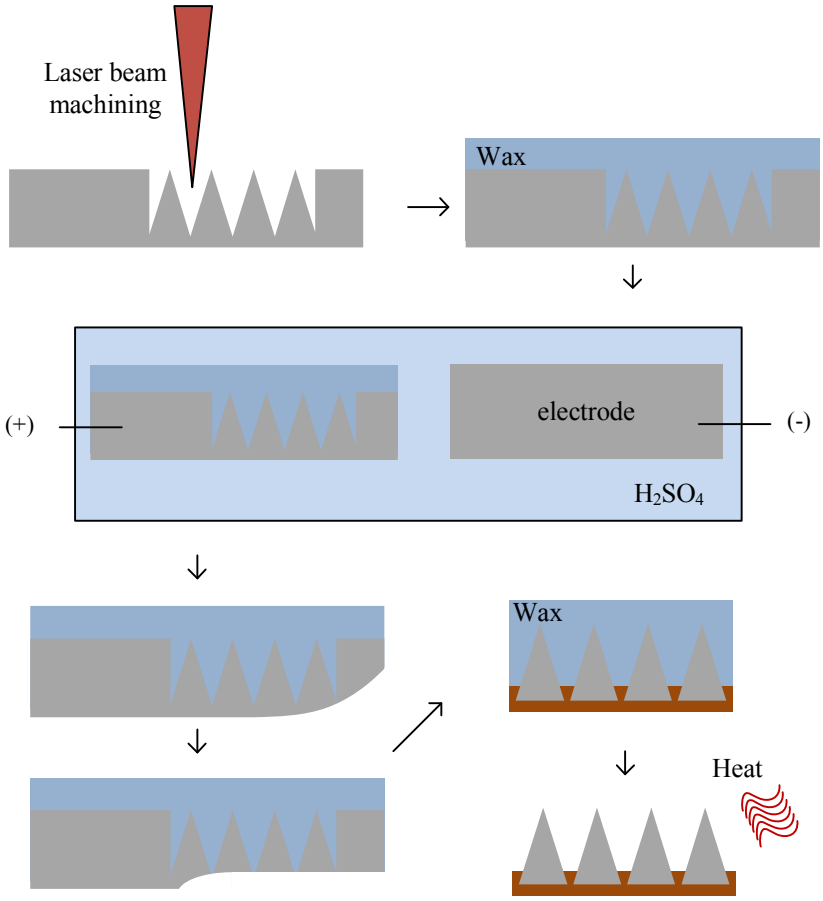

Figure 5.6 Schematic procedure to fabricate micro-pin array with flexible base using laser beam machining and electrochemical etching

Interlocking force of flexible base micro-pin array was measured on flat and curved surface. The radius of curved surface was 36.0 mm. Both flat and curved surface was covered by 400 grit sandpaper. Measurement results were shown in table 5.1. Since elasticity of flexible base can endure less force than metal base, interlocking force of general micro-pin array was more than flexible base micro-pin array on flat surface. On the other hand, flexible base micro-pin array generated more interlocking force on curved surface than general micro-pin array. General and flexible base micro-pin arrays showed force degradation on curved surface. In degradation rate aspect, flexible base micro-pin array was better than general micro-pin array. Flexible base micro-pin array could maintain contact area using flexibility of base.

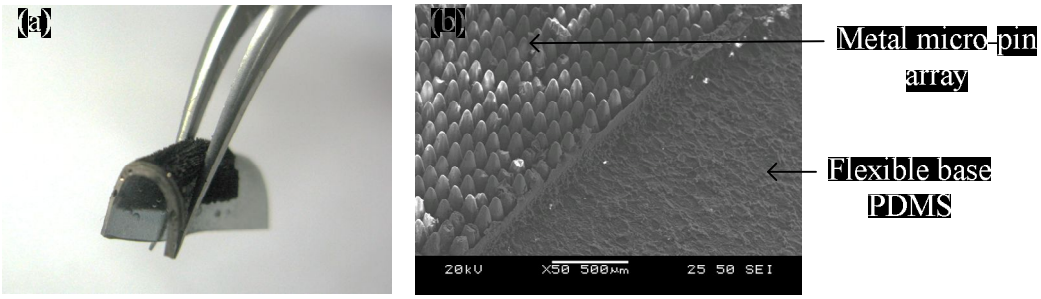

Figure 5.7 Fabricated micro-pin array with flexible base: (a) deformation by outside force, (b) SEM image of flexible base micro-pin array

Table 5.1 Interlocking force of micro-pin array on flat and curved surface

	General micro-pin array	Flexible base micro-pin array
On flat surface	0.696 g/mm^2	0.565 g/mm^2
On curved surface	0.141 g/mm^2	0.450 g/mm^2

Chapter 6

Conclusion

Micro-pin array for interlocking on rough surface was fabricated on metal surface. To fabricate micro-pin array on large area effectively, nano second pulsed laser beam machining was applied. Different machining process for micro-pin array was proposed according to machining characteristics of workpiece material.

On stainless steel that forms much recast layer and dross, recast layer piling was applied. Recast layer and dross were the by-product that decreased machining efficiency. But in this study, micro-pin array was fabricated using recast layer and dross. For recast layer piling, laser beam machining system was set up and machining parameter investigation was carried out.

On tungsten that has high thermal conductivity, laser beam machining and electrochemical etching were carried out sequentially. Since unidirectional laser beam scanning caused material flow within molten metal pool, asymmetric distribution of recast layer appeared. This led incomplete and unbalanced

electrochemical etching of micro-pin array. To solve this problem, laser beam scanning sequence was adjusted and micro-pin array was fabricated successfully on tungsten. For efficient machining, machining parameter investigations about laser beam machining and electrochemical machining were carried out.

Micro-pin array was applied to interlocking on rough surface. Especially, it can be attached to vertical rough surface using interlocking force. Principle of interlocking was also studied. Pin – surface interlocking model was proposed. Interlocking model was regarded as inclined plane and whole model could be simplified as the friction model on the inclined plane. Interlocking model was established and verification of the model was carried out by comparison between modeling result and actual force measurement. In addition, force estimation based on the established model was carried out using surface profile investigation. In this process, meaningful slope angle was extracted. The points of high contact angle were excepted and bending deformation of micro-pin was considered. After all, interlocking force could be estimated.

Applications of micro-pin array were developed for improve interlocking performances. To improve interlocking force, tilted micro-pin array was fabricated. In fabrication process, focal length should be considered. To solve this problem height of laser beam source was adjusted in sync with machining part on tilted workpiece. As a result, tilted micro-pin array was fabricated and it generated more

and directional force than general micro-pin array. To maintain contact area on curved surface, flexible base micro-pin array was fabricated. To remove original metal base, electrochemical etching using sulfuric acid was applied. And it was displaced by PDMS base. Flexible base micro-pin array could maintain contact area on curved surface and it showed better interlocking performance than general micro-pin array.

References

[1] J. Vangelooven, G. Desmet, Theoretical optimisation of the side-wall of micropillar array columns using computational fluid dynamics, J. Chromatogr. A, 1217 (2010) 8121-8126.

[2] J. Op de Beeck, W. De Malsche, J. Vangelooven, H. Gardeniers, G. Desmet, Hydrodynamic chromatography of polystyrene microparticles in micropillar array columns, J. Chromatogr. A, 1217 (2010) 6077-6084.

[3] S. Yi, K.S. Seo, Y.H. Cho, A DNA trapping and extraction microchip using periodically crossed electrophoresis in a micropillar array, Sens. Actuator A-Phys., 120 (2005) 429-436.

[4] J.R. Maiolo, B.M. Kayes, M.A. Filler, M.C. Putnam, M.D. Kelzenberg, H.A. Atwater, N.S. Lewis, High aspect ratio silicon wire array photoelectrochemical cells, J. Am. Chem. Soc., 129 (2007) 12346-+.

[5] D. Oner, T.J. McCarthy, Ultrahydrophobic surfaces. Effects of topography length scales on wettability, Langmuir, 16 (2000) 7777-7782.

[6] G. La Rosa, M. Messina, G. Muscato, R. Sinatra, A low-cost lightweight climbing robot for the inspection of vertical surfaces, Mechatronics, 12 (2002) 71-96.

[7] K. Wang, W. Wang, H. Zhang, Analysis and Design of Attachment Module Based on Sine Vibrating Suction Method for Wall-climbing Robot, Procedia Engineering, 12 (2011) 9-14.

[8] K.A. Daltorio, T.E. Wei, A.D. Horchler, L. Southard, G.D. Wile, R.D. Quinn, S.N. Gorb, R.E. Ritzmann, Mini-Whegs TM Climbs Steep Surfaces Using Insect-inspired Attachment Mechanisms, The International Journal of Robotics Research, 28 (2009) 285-302.

[9] A. Sintov, T. Avramovich, A. Shapiro, Design and motion planning of an autonomous climbing robot with claws, Robot. Auton. Syst., 59 (2011) 1008-1019.

[10] A.T. Asbeck, S. Kim, M.R. Cutkosky, W.R. Provancher, M. Lanzetta, Scaling hard vertical surfaces with compliant microspine arrays, Int. J. Robot. Res., 25 (2006) 1165-1179.

[11] S. Thrun, G.S. Sukhatme, S. Schaal, Robotics: Science and Systems I, first ed., MIT Press, Massachusetts, 2005.

[12] C. Balaguer, A. Gimenez, J.M. Pastor, V.M. Padron, C. Abderrahim, A climbing autonomous robot for inspection applications in 3D complex environments, Robotica, 18 (2000) 287-297.

[13] S. Kim, M. Spenko, S. Trujillo, B. Heyneman, D. Santos, M.R. Cutkosky, Smooth vertical surface climbing with directional adhesion, IEEE Trans. Robot., 24 (2008) 65-74.

[14] D. Santos, M. Spenko, A. Parness, S. Kim, M. Cutkosky, Directional adhesion for climbing: theoretical and practical considerations, J. Adhes. Sci. Technol., 21 (2007) 1317-1341.

[15] G. Lee, G. Wu, J. Kim, T. Seo, High-payload climbing and transitioning by compliant locomotion with magnetic adhesion, Robot. Auton. Syst., 60 (2012) 1308-1316.

[16] Z.D. Dai, S.N. Gorb, U. Schwarz, Roughness-dependent friction force of the tarsal claw system in the beetle Pachnoda marginata (Coleoptera, Scarabaeidae), J. Exp. Biol., 205 (2002) 2479-2488.

[17] X. Li, H.S. Seo, H.D. Um, S.W. Jee, Y. Cho, B. Yoo, J.H. Lee, A periodic array of silicon pillars fabricated by photoelectrochemical etching, Electrochimica Acta, 54 (2009) 6978-6982.

[18] C. Padeste, H. Ozcelik, J. Ziegler, A. Schleunitz, M. Bednarzik, D. Yucel, V. Hasirci, Replication of high aspect ratio pillar array structures in biocompatible polymers for tissue engineering applications, Microelectron. Eng., 88 (2011) 1836-1839.

[19] L. Sainiemi, H. Keskinen, M. Aromaa, L. Luosujarvi, K. Grigoras, T. Kotiaho, J.M. Makela, S. Franssila, Rapid fabrication of high aspect ratio silicon nanopillars for chemical analysis, Nanotechnology, 18 (2007).

[20] D.K. Chung, H.S. Shin, M.S. Park, B.H. Kim, C.N. Chu, Recent Researches in Micro Electrical Machining, Int. J. Precis. Eng. Manuf., 12 (2011) 371-380.

[21] D.K. Chung, H.S. Shin, M.S. Park, C.N. Chu, Machining Characteristics of Micro EDM in Water using High Frequency Bipolar Pulse, Int. J. Precis. Eng. Manuf., 12 (2011) 195-201.

[22] E.S. Lee, J.K. Won, T.H. Shin, S.H. Kim, Investigation of Machining Characteristics for Electrochemical Micro-Deburring of the AZ31 Lightweight Magnesium Alloy, Int. J. Precis. Eng. Manuf., 13 (2012) 339-345.

[23] D. Starikov, C. Boney, R. Pillai, A. Bensaoula, G.A. Shafeev, A.V. Simakin, Spectral and surface analysis of heated micro-column arrays fabricated by laser-assisted surface modification, Infrared Phys. Technol., 45 (2004) 159-167.

[24] W.M. Steen, J. Mazumder, Laser Material Processing, 4th edition ed., Springer, London, 2010.

[25] N.B. Dahotre, Lasers in Surface engineering, ASM International, Canada, 1998.

[26] D.H. Kim, Laser Processing, Kyungmoonsa, Seoul, 2005.

[27] K.A. Ghany, M. Newishy, Cutting of 1.2 mm thick austenitic stainless steel sheet using pulsed and CWNd : YAG laser, J. Mater. Process. Technol., 168 (2005)

438-447.

[28] A. Riveiro, F. Quintero, F. Lusquinos, R. Comesana, J. Pou, Study of melt flow dynamics and influence on quality for CO2 laser fusion cutting, J. Phys. D-Appl. Phys., 44 (2011).

[29] G. Tani, L. Tomesani, G. Campana, A. Fortunato, Quality factors assessed by analytical modelling in laser cutting, Thin Solid Films, 453 (2004) 486-491.

[30] B.S. Yilbas, B.J.A. Aleem, Dross formation during laser cutting process, J. Phys. D-Appl. Phys., 39 (2006) 1451-1461.

[31] S. Kim, B.H. Kim, D.K. Chung, H.S. Shin, C.N. Chu, Hybrid micromachining using a nanosecond pulsed laser and micro EDM, J. Micromech. Microeng., 20 (2010).

[32] M.R.H. Knowles, G. Rutterford, D. Karnakis, A. Ferguson, Micro-machining of metals, ceramics and polymers using nanosecond lasers, Int. J. Adv. Manuf. Technol., 33 (2007) 95-102.

[33] J.C. Aurich, D. Dornfeld, P.J. Arrazola, V. Franke, L. Leitz, S. Min, Burrs-Analysis, control and removal, CIRP Ann-Manuf. Technol., 58 (2009) 519-542.

[34] T. Dobrev, D.T. Phain, S.S. Dimov, Techniques for improving surface quality after laser milling, Proc. Inst. Mech. Eng. Part B-J. Eng. Manuf., 222 (2008) 55-65.

[35] H.K. Tönshoff, D. Hesse, J. Mommsen, Micromachining Using Excimer Lasers, CIRP Annals - Manufacturing Technology, 42 (1993) 247-251.

[36] H. Zhang, J.W. Xu, J.S. Zhao, G.R. Hua, Mechanism of Recast Removal During Laser Drilling Underwater, Adv. Sci. Lett., 4 (2011) 2071-2075.

[37] C. Madore, D. Landolt, Electrochemical micromachining of controlled topographies on titanium for biological applications, J. Micromech. Microeng., 7 (1997) 270-275.

[38] G.J. Kwon, H.Y. Sun, H.J. Sohn, WALL PROFILE DEVELOPMENTS IN THROUGH-MASK ELECTROCHEMICAL MICROMACHINING OF INVAR ALLOY-FILMS, J. Electrochem. Soc., 142 (1995) 3016-3020.

[39] C. Chan, J. Mazumder, M.M. Chen, A TWO-DIMENSIONAL TRANSIENT MODEL FOR CONVECTION IN LASER MELTED POOL, Journal of Metals, 35 (1983) 49-49.

국문 초록

본 논문에서는 거친 표면에 인터로크를 위한 금속 미세 핀 배열의 가공 방법에 대한 연구를 진행하였다. 대면적 가공에 유리한 나노초 펄스 레이저 빔을 미세 핀 배열에 적용하였고, 금속의 레이저 빔 가공 특성에 따라 적절한 가공법을 제시하였다. 스테인리스강과 같이 용융 금속의 점도 및 표면장력이 크고, 레이저 빔 가공 중에 발생하는 드로스 (dross)로 인해 재응고층이 많은 금속의 경우, 생성되는 드로스와 재응고층을 쌓아 고세장비의 미세 핀 배열을 가공하였다. 텅스텐과 같이 녹는점, 열전도율이 높아 레이저 빔 가공을 통한 정밀 미세 가공이 어려운 금속에 대해서는 레이저 빔 가공을 한 후 전해 에칭을 통해 미세 핀 배열을 가공하였다. 또한 제시한 가공 방법에 따라 알맞은 가공 조건을 선정하였다.

가공한 미세 핀 배열을 이용하여 거친 표면 인터로크에 적용하였다. 미세 핀의 형상과 거친 표면의 조건에 따라 인터로크에 의해 발생하는 힘을 측정하였다. 또한 본 논문에서는 미세 핀 배열을 이용한 거친 표면 인터로크의 원리를 분석하였다. 인터로크 모델과 실제 발생 힘의 비교하였고, 이를 통하여 표면 프로파일을 이용한 인터로크 힘 예측을 수행하였다. 또한 미세 핀 배열을 이용한 인터로크의 다양한 응용을 위하여 tilted 미세 핀 배열과 연성 기반의

미세 핀 배열을 제안하고 그 가공 방법을 개발하였다. Tilted 미세 핀 배열을 이용하여 방향성을 갖지만 더 큰 인터로크 힘을 발생시킬 수 있었고, 연성 기반의 미세 핀 배열을 이용하여 곡면에서도 인터로크가 가능하게 할 수 있었다.

주요어: 금속 미세 핀 배열, 정밀 가공, 레이저 빔 가공, 전해 에칭, 인터로크, 거친표면

학번: 2006 – 23098

Ph. D Dissertation Information

Submitted to the School of Mechanical and Aerospace Engineering and the Committee on Graduate Studies of Seoul National University in Partial Fulfillment of the Requirements for the Degree of Doctor of Philosophy

Title: Fabrication of Metal Micro-pin Array for Mechanical Interlocking on Rough Surface
Keywords: Metal micro-pin array, Precise machining, Laser beam machining, Electrochemical machining, Interlocking, Rough surface.

Author: Se Won Lee
Advisor: Professor Chong Nam Chu
Laboratory: Precision Engineering & Manufacturing Lab., Seoul National University
Contact: nowes0@snu.ac.kr, http://prema.snu.ac.kr

Version: Final
Date: February 5, 2014